

A Bayesian Gaussian Process Dynamic Factor Model

Tony CHERNIS*

Bermuda Monetary Authority

Haroon MUMTAZ

Queen Mary University of London

Niko HAUZENBERGER

University of Strathclyde

Michael PFARRHOFFER

WU Vienna

Abstract

We propose a dynamic factor model (DFM) where the latent factors are linked to observed variables with unknown and potentially nonlinear functions. The key novelty and source of flexibility of our approach is a nonparametric observation equation, specified via Gaussian Process (GP) priors for each series. Factor dynamics are modeled with a standard vector autoregression (VAR), which facilitates computation and interpretation. We discuss a computationally efficient estimation algorithm and consider two empirical applications. First, we forecast key series from the FRED-QD dataset and show that the model yields improvements in predictive accuracy relative to linear benchmarks. Second, we extract driving factors of global inflation dynamics with the GP-DFM, which allows for capturing international asymmetries.

JEL Classification: C11; C32; C55; E17; E31.

Keywords: Nonlinear state space models; Big data; Machine learning; Macroeconomic forecasting; Inflation dynamics.

Corresponding author: Haroon Mumtaz (h.mumtaz@qmul.ac.uk). We thank Annika Camehl, Yizhou Kuang, Michele Lenza, and Aubrey Poon, as well as the participants of the *Advances in Macroeconometrics Workshop* in Manchester and the *IAAE 2025* in Turin. Hauenberger acknowledges funding by the Jubiläumsfonds of the OeNB, grant no. 18763.

* The views expressed in this paper are solely those of the authors and may differ from the views of the Bermuda Monetary Authority. No responsibility for them should be attributed to the Bermuda Monetary Authority.

1. INTRODUCTION

Nonlinearities are an important feature of macroeconomic and financial data. In just the last decade, the Global Financial Crisis, COVID-19 pandemic, and central banks reaching their effective lower bound provide examples. Capturing these nonlinearities has become an increasingly important issue—there is widening recognition that they are important for understanding and predicting macroeconomic dynamics.¹

In addition to the focus on modeling various forms of nonlinearities, a key feature of modern macroeconometric approaches is their scalability to high-dimensional datasets. These days it is straightforward to download hundreds of macroeconomic time series with a single click; examples for datasets include the US-based FRED-MD/QD (McCracken and Ng, 2016; 2021), or other well-maintained multi-country databases. Exploiting macroeconomic “Big Data” (which typically involves many variables and few observations) to improve structural analysis and forecasting, and, consequently, policymaking, is a focus of researchers and practitioners alike; see Bok *et al.* (2018) for a recent review. And while there is no obvious best way to econometrically model these data (Giannone *et al.*, 2021), there is a popular front-runner—the dynamic factor model (DFM).

DFMs are a workhorse model of empirical macroeconomics (see, e.g., Aguilar and West, 2000; Forni *et al.*, 2000; Stock and Watson, 2002; Kose *et al.*, 2003; Giannone *et al.*, 2008; Chernis and Sekkel, 2017; Kaufmann and Schumacher, 2019).² A DFM assumes that there are a few fundamental forces in the economy which explain common dynamics of many time series. These fundamental forces (or latent factors) are usually modeled using a vector autoregression (VAR). A DFM thus compresses the data to work with a

¹ For example, a broad strand of literature on macro-financial linkages (e.g., Brunnermeier and Sannikov, 2014; Adrian *et al.*, 2019) or the Phillips curve (e.g., Hamilton, 2001; Beaudry *et al.*, 2024; Ball *et al.*, 2022; Benigno and Eggertsson, 2023) documents instability in the underlying (structural) relationships. This is consequential for effective policy analysis and policy making. Modeling nonlinearities generally has a long tradition in macroeconometrics, with competing approaches ranging from regime-switching (e.g., Hamilton, 1989; Teräsvirta, 1994; Sims and Zha, 2006) to time-varying parameter (TVP, e.g., Primiceri, 2005; Cogley and Sargent, 2005; Koop and Korobilis, 2013) models.

² Stock and Watson (2016) and Doz and Fuleky (2020) provide excellent surveys of the earlier literature.

more parsimonious VAR, rather than shrinking a large VAR featuring many variables towards a simpler specification, another popular option (see Bańbura *et al.*, 2010).

Despite the overall popularity of (linear) DFMs, few papers model any nonlinear relationships between factors and observable variables. As we pointed out above, these may indeed be crucial to understand major macroeconomic fluctuations. Exceptions include DFMs with time-varying loadings (Del Negro and Otrok, 2008; Mumtaz and Surico, 2012; Korobilis, 2013; Zhou *et al.*, 2014), or DFMs with Markov-switching dynamics (Chauvet, 1998; Chauvet and Senyuz, 2016; Camacho *et al.*, 2018). More recently nonlinear DFMs with a squared/quadratic dynamics in the measurement or state equation (Guerrón-Quintana *et al.*, 2023) have been proposed. However, these studies impose specific functional forms in the context of inferring the latent factors.³ In other words, they impose explicit restrictions on the link between the factors and observed variables.

Machine learning techniques have proven useful for modeling nonlinearities of unknown form in big macroeconomic datasets.⁴ These techniques are appealing for several reasons. First, machine learning approaches are flexible and only require mild assumptions about the form of nonlinearities. Second, these methods are designed to avoid oversimplification, misspecification, and overfitting. Third, these sophisticated methods are well-suited for learning and identifying common patterns in large datasets, enabling efficient information extraction.

This paper introduces a general nonlinear DFM and develops a computationally feasible and fully Bayesian estimation algorithm. As mentioned above, imposing linearity in a typical DFM may be too restrictive, and we thus relax this assumption. Specifically, we propose to use Gaussian processes (GPs, Williams and Rasmussen, 2006), to obtain

³ An exception is Velasco (2024) who uses Bayesian Additive Regression Trees (BART) to model nonlinearities in a DFM. Unlike our approach, she employs a linear approximation to the relationship when estimating the factors. Another related approach is Clark *et al.* (2025), who by contrast use a VAR augmented with static nonlinear factors modeled via BART.

⁴ An incomplete list of examples includes Bassetti *et al.* (2014), Kalli and Griffin (2018), Farrell *et al.* (2021), Medeiros *et al.* (2021), Babii *et al.* (2022), Goulet Coulombe *et al.* (2022), Jin *et al.* (2022), Huber *et al.* (2023), Clark *et al.* (2024b), Chronopoulos *et al.* (2024), Goulet Coulombe (2024), Hauzenberger *et al.* (2024a,b, 2025).

a nonparametric Gaussian Process Dynamic Factor Model (GP-DFM). GPs can capture a wide range of possible nonlinear relationships between latent (or observed) factors and high-dimensional data, and they have a successful track record in macroeconomic modeling (Clark *et al.*, 2024a; Hauzenberger *et al.*, 2025). Compared with other recent nonlinear DFM approaches, our approach is more flexible as this novel framework does not impose any specific type of nonlinearity. Instead, we place a prior (which is compatible with a rich menu of functions, and governed by a distance-based kernel function subject to only a few tuning parameters) directly on the functional relationship between common latent factors and the observed series.

Part of our contribution is bridging the machine learning literature on Gaussian Processes with macroeconometrics in a Big data context (where sample sizes are typically rather small). Specifically, we use GPs in a state space framework (Turner *et al.*, 2010; Frigola *et al.*, 2013). The main novelty of our framework lies in the nonlinear and flexible treatment of the measurement equation, while the state equation is assumed to follow a standard linear VAR. From both a practical and forecasting perspective, the use of a linear VAR in the state equation offers several appealing features.

First, interpretation of the latent common factors is analogous to a standard linear DFM. So, conventional tools from structural and reduced form VAR analysis can be readily used to the linear VAR in the state equation—for example, to produce forecasts as well as impulse response functions (IRFs) for the latent factors quickly. Once the full paths of these forecasts and the IRFs of the factors are known, the nonlinear mapping between observables and latent factors in the measurement equation can be exploited to generate forecasts or IRFs for the observed time series. This treatment results in the ability to calculate structural and reduced form quantities that can be time-varying or state dependent.

Second, this modeling strategy can also be viewed as a form of nonlinear dimension reduction, where high-dimensional macroeconomic data are assumed to lie on a lower-dimensional manifold or space. Any nonlinearity in the model arises exclusively from the relationship between the latent factors and the observables, which captures the no-

tion of providing a more accurate/precise description of the variation in a large panel of time series. There is a relationship to other dimension reduction techniques such as local linear manifold regression (Cheng and Wu, 2013), nonlinear principal components (PCs, Bai and Ng, 2008), deep/nonlinear dynamic factor models and autoencoders, which use neural networks to uncover complex patterns in high-dimensional data (Andreini *et al.*, 2023; Hauzenberger *et al.*, 2023; Guerrón-Quintana *et al.*, 2023; Klieber, 2024; Snellman, 2024; Luo *et al.*, 2025). However, unlike existing deep dynamic factor model approaches and popular two-stage procedures, our GP-DFM offers a fully consistent modeling framework. At its core, it represents a Bayesian state space model in which the functional relationship between low-dimensional latent factors and high-dimensional observables is explicitly modeled, with parameters and latent processes with precisely defined priors and posteriors. These posteriors are jointly estimated using a Markov Chain Monte Carlo (MCMC) algorithm (which is part of the contribution of this paper). This framework ensures both model consistency and proper Bayesian uncertainty quantification for all parameters and latent processes in the model, the latter being important for obtaining accurate predictive densities (see Geweke and Amisano, 2010).

A fully nonlinear measurement equation is challenging to estimate, as it requires computationally intensive particle filtering techniques. To facilitate Bayesian estimation and provide a computationally feasible option for inference, we use the algorithm proposed in Svensson *et al.* (2016). This framework involves a linear approximation of the GP using basis functions derived from the spectral densities of the GP kernels (Solin and Särkkä, 2020). In addition, we rely on Particle Gibbs with Ancestor Sampling (PGAS) inspired by Lindsten *et al.* (2014), which greatly improves the efficiency of our algorithm. We further improve computational scalability by proposing an alternative parameterization of the GP kernel that uses an additive structure instead of a multiplicative one. This approach sacrifices some flexibility because it restricts interactions between the factors in the measurement equations, but there are significant computational advantages to this specification. Finally, since our approach uses a fully Bayesian MCMC algorithm, we can

straightforwardly implement key model features such as stochastic volatility and shrinkage priors for the VAR process governing the state dynamics.

We provide two different empirical applications. In our first application, we forecast key macroeconomic variables from the FRED-QD dataset. The GP-DFM outperforms linear specifications of the DFM—a workhorse model at many policy institutions. Some of the superior performance is due to the GP-DFM forecasting real activity variables well during the COVID-19 period and the Federal funds rate when it is close to the effective lower bound. Interestingly, we find that with the nonlinear GP-DFM, a smaller number of factors is sufficient to extract the high-dimensional information than when imposing linearity. This supports the notion that in large macroeconomic datasets nonlinear factors can capture richer dynamics than their linear counterparts, which require more components to achieve comparable accuracy. In our second application, we measure international inflation dynamics with GP-DFM, and study nonlinearities and asymmetries arising from shocks to the global component of inflation in a large cross-section of economies.

The rest of the paper is structured as follows. Section 2 lays out the econometric framework. This includes the DFM, GP priors subject to computationally favorable kernel specifications, and the posterior and predictive sampling algorithm. Section 3 applies the GP-DFM in a forecast horserace with US data, while in Section 4 we use the model to capture nonlinearities in international inflation dynamics. Section 5 concludes.

2. ECONOMETRIC FRAMEWORK

2.1. A Gaussian process dynamic factor model (GP-DFM)

A general nonlinear DFM relates N observed macroeconomic time series (measurements), $\mathbf{y}_t = (y_{1t}, \dots, y_{Nt})'$, to a set of D common latent factors $\mathbf{f}_t = (f_{1t}, \dots, f_{Dt})'$:

$$\mathbf{y}_t = \mathbf{G}(\mathbf{f}_t) + \mathbf{v}_t, \quad \mathbf{v}_t \sim \mathcal{N}(\mathbf{0}_N, \mathbf{R}). \quad (1)$$

Equation (1) is a measurement equation, where an unknown function $\mathbf{G}(\bullet) : \mathbb{R}^D \rightarrow \mathbb{R}^N$ maps latent inputs \mathbf{f}_t to observed outputs \mathbf{y}_t . In the following, we assume $\mathbf{G}(\mathbf{f}_t) = (g_1(\mathbf{f}_t), \dots, g_N(\mathbf{f}_t))'$ collects equation-specific functions, with $g_i(\bullet) : \mathbb{R}^D \rightarrow \mathbb{R}$, for $i = 1, \dots, N$. The idiosyncratic component \mathbf{v}_t is Gaussian distributed with zero mean and variance-covariance matrix $\mathbf{R} = \text{diag}(r_1, \dots, r_N)$. While $\mathbf{G}(\mathbf{f}_t)$ captures variation common to all time series in \mathbf{y}_t , \mathbf{v}_t is specific to each time series. Moreover, flexible equation-specific functions allow the common factors \mathbf{f}_t to affect each variable differently, adequately reflecting the idea that different time series may feature different types of nonlinearities, captured by possibly different functional forms of g_i .

The nonlinear measurement equation is combined with a linear state equation for the factors, which follow a joint VAR(P) process:⁵

$$\mathbf{f}_t = \sum_{p=1}^P \mathbf{A}_p \mathbf{f}_{t-p} + \boldsymbol{\varepsilon}_t, \quad \boldsymbol{\varepsilon}_t \sim \mathcal{N}(\mathbf{0}_D, \mathbf{Q}), \quad (2)$$

with coefficient matrices $\mathbf{A} = (\mathbf{A}_1, \dots, \mathbf{A}_P)$ that relate \mathbf{f}_t to their P lags. In addition, $\boldsymbol{\varepsilon}_t = (\varepsilon_{1t}, \dots, \varepsilon_{Dt})'$ are zero mean state innovations with variance-covariance matrix \mathbf{Q} .⁶

In terms of features of this general framework, a few considerations are noteworthy. Eqs. (1) and (2) define a state space model. Specifically, \mathbf{f}_t can be viewed as a lower dimensional representation of the high-dimensional data \mathbf{y}_t , which strikes a balance between explaining most of the variation in the data and parsimony. In this regard, a critical assumption is $D \ll N$.

⁵ Note that more general multivariate processes, e.g., $\mathbf{f}_t = \mathbf{H}(\mathbf{f}_{t-1}, \dots, \mathbf{f}_{t-p}) + \boldsymbol{\varepsilon}_t$, can and have been used as state equations in nonlinear state space models (e.g., Frigola *et al.*, 2013; Guerrón-Quintana *et al.*, 2023); see Marcellino and Pfarrhofer (2024) for a recent review of the macroeconomic literature using such models with (observed) macro-data. For the reasons we outlined in the Introduction (i.e., striking a balance between flexibility, computational efficiency, general ease of use and interpretability), we impose that $\mathbf{H}(\bullet)$ is linear a priori and leave nonlinear extensions for future research.

⁶ In the empirical application, we also investigate whether allowing for stochastic volatility (SV), with a time-varying \mathbf{Q}_t rather than a constant \mathbf{Q} , improves forecast accuracy (see Clark, 2011; Clark and Ravazzolo, 2015).

A standard DFM assumes a linear mapping, $\mathbf{G}(\mathbf{f}_t) = \mathbf{\Lambda}\mathbf{f}_t$, with $\mathbf{\Lambda}$ being an $N \times D$ loadings matrix. In such a case, Eqs. (1) and (2) resemble a Gaussian linear state space model and for estimation standard algorithms such as forward sampling backward smoothing (FFBS, [Carter and Kohn, 1994](#); [Frühwirth-Schnatter, 1994](#)) or the precision sampler ([Chan and Jeliazkov, 2009](#)) can be used. However, this linearity assumption may be too restrictive and is an assumption we wish to relax. To do so, one might consider incorporating nonlinear features, e.g., of the form $\phi(\mathbf{f}_t) = (\mathbf{f}'_t, (\mathbf{f}_t \odot \mathbf{f}_t)')'$; a related approach is discussed in [Guerrón-Quintana *et al.* \(2023\)](#).

Related to this so-called “feature space” (see [Williams and Rasmussen, 2006](#), chapter 2) two points are worth highlighting. First, $\phi(\mathbf{f}_t) = (\mathbf{f}'_t, (\mathbf{f}_t \odot \mathbf{f}_t)')'$, or other simple transformations, would denote a deterministic projection of \mathbf{f}_t onto $\phi(\mathbf{f}_t)$. However, we use a general form for $\phi(\mathbf{f}_t)$ which, by virtue of being more flexible, can approximate deterministic transforms but does not require knowing the appropriate transform ahead of time. Second, recall \mathbf{f}_t is latent. Hence, any $\phi(\mathbf{f}_t)$ that includes nonlinear transforms of \mathbf{f}_t leads to a nonlinear state space model, for which standard sampling algorithms can no longer be used. In short, our approach does not require pre-specifying the form of nonlinearity and we provide an estimation algorithm which is feasible for nonlinear measurement equations. The remaining sub-sections of the econometric framework will focus on these two considerations and carefully outline the contribution of this paper.

2.2. Gaussian processes (GPs) as the measurement equation

The key innovation of our model is the measurement equation features unknown nonlinearities. We choose GPs since they have a proven track record in macroeconomic (and many other) applications, and because of several properties that will result in a computationally feasible estimation algorithm. The key feature of GPs is that they model the covariance between observations through a simple kernel function. Kernel functions usually only have few parameters, but they are very expressive. Despite their sparse parametrization, GPs can indeed approximate a wide variety of functions.⁷

⁷ There are theoretical equivalencies between neural nets and GPs ([Neal, 1996](#); [Lee *et al.*, 2018](#)).

We begin describing the model, starting with the i^{th} measurement equation:

$$y_{it} = g_i(\mathbf{f}_t) + v_{it}, \quad v_{it} \sim \mathcal{N}(0, r_i).$$

We assume a GP prior on each observable-specific function:

$$g_i(\mathbf{f}_t) \sim \mathcal{GP}(0, \mathcal{K}_i(\mathbf{f}_t, \mathbf{f}_t)), \quad (3)$$

where $\mathcal{K}_i(\bullet)$ is a suitable covariance function (called the kernel) which we define below. Eq. (3) denotes a prior over all possible functions g_i that fit the i^{th} equation well, without explicitly taking a stance of the functional form of g_i and thus the feature space of \mathbf{f}_t . Through an appropriate choice of kernel we can allow for an infinite set of basis functions and feature space $\phi(\mathbf{f}_t)$. This means a GP can approximate any arbitrary continuous function, see also [Williams and Rasmussen \(2006\)](#).

This paper focuses on two distinct versions of the commonly used squared exponential kernel. One variant is multiplicative across covariates and the other additive:

$$\mathcal{K}_{i,M}(\mathbf{f}_t, \mathbf{f}_\tau) = \xi_i \cdot \prod_{j=1}^D \exp \left(-\frac{1}{2} \frac{(f_{jt} - f_{j\tau})^2}{\ell_{ij}^2} \right) \quad (4a)$$

$$\mathcal{K}_{i,A}(\mathbf{f}_t, \mathbf{f}_\tau) = \xi_i \cdot \sum_{j=1}^D \exp \left(-\frac{1}{2} \frac{(f_{jt} - f_{j\tau})^2}{\ell_{ij}^2} \right), \quad (4b)$$

with hyperparameters $\boldsymbol{\theta}_i = (\xi_i, \{\ell_{ij}\}_{j=1}^D)'$ defining covariances between two periods t and τ . Here, ξ_i denotes an unconditional variance parameter and $\{\ell_{ij}\}_{j=1}^D$ refer to factor-specific length scales. We label the former variant in Eq. (4a) the multiplicative (**multi**) GP-DFM, and the latter in Eq. (4b) the additive (**hybrid**) GP-DFM. Both variants define a stationary covariance function appropriate for macroeconomic data. However, they differ in the interactions between inputs (factors). The additive kernel sums the squared exponential terms instead of multiplying them. This difference has implications for computation and modeling flexibility, which we discuss in more detail below.

In the following, we first discuss the implications of GPs with a generic stationary kernel in the measurement Eq. (1). If \mathbf{f}_t were known, this would denote an otherwise standard GP regression, with inference being straightforward. However, \mathbf{f}_t is latent which substantially complicates estimation and inference. To see this, define $\mathbf{g}_i = (g_i(\mathbf{f}_1), \dots, g_i(\mathbf{f}_T))'$, then the GP takes the form:

$$\mathbf{g}_i \sim \mathcal{N}(\mathbf{0}_T, \mathcal{K}_i(\mathbf{F}, \mathbf{F}')),$$

with $\mathcal{K}_i(\mathbf{f}_t, \mathbf{f}_\tau)$ being the $(t, \tau)^{\text{th}}$ entry in $\mathcal{K}_i(\mathbf{F}, \mathbf{F}')$. Considering the weight-space view of our GP model in the i^{th} equation, we obtain:

$$\mathbf{y}_i = \mathbf{W}_i \boldsymbol{\eta}_i + \mathbf{v}_i, \quad \boldsymbol{\eta}_i \sim \mathcal{N}(\mathbf{0}, \mathbf{I}_T).$$

Here, \mathbf{W}_i denotes the lower Cholesky factor of $\mathcal{K}_i(\mathbf{F}, \mathbf{F}') = \mathbf{W}_i \mathbf{W}_i'$, with $w_{i,t\tau}$ referring to the $(t, \tau)^{\text{th}}$ element of \mathbf{W}_i . Note that $\mathcal{K}_i(\mathbf{F}, \mathbf{F}')$ denotes a full (symmetric) $T \times T$ variance-covariance matrix, implying that the measurement equation relates y_{it} to the full history of latent states \mathbf{f}_t :

$$y_{it} = \sum_{\tau=1}^t w_{i,t\tau} \eta_{i\tau} + v_{it}. \tag{5}$$

As alluded to by the weight space view, the measurement equation is rather involved, rendering a fully Bayesian approach feasible but computationally cumbersome (see, e.g., Frigola *et al.*, 2013).

2.3. Reduced-rank approximation of the GP

In our paper, we approximate the GP using a set of nonlinear basis functions. These basis functions are based on the spectral density of the kernels in Eq. (4), see Svensson *et al.* (2016), Solin and Särkkä (2020), Riutort-Mayol *et al.* (2023). Loosely speaking, this facilitates estimation by breaking the dependence on the full history of latent factors $\{\mathbf{f}_\tau\}_{\tau=1}^t$, relying instead only on transformations of \mathbf{f}_t . In general, this approximation is

enabled by the fact that any stationary covariance function can be represented in terms of their spectral densities $\mathcal{S}_i(\boldsymbol{\omega})$. Using eigenfunction expansion, any stationary covariance function with inputs \mathbf{f}_t can then be expressed as:

$$\mathcal{K}_i(\mathbf{f}_t, \mathbf{f}_\tau) = \sum_{m=1}^{\infty} \mathcal{S}_i(\sqrt{\boldsymbol{\lambda}_m}) \phi_m(\mathbf{f}_t) \phi_m(\mathbf{f}_\tau), \quad (6)$$

with \mathcal{S}_i denoting the spectral density, $\boldsymbol{\lambda}_m$ are vectors of eigenvalues and $\phi_m(\mathbf{f}_t)$ are eigenfunctions of the Laplacian operator that is used to establish the approximation in domain Ω . More formally, $\Omega \in [-L_1, L_1] \times \dots \times [-L_D, L_D]$ (i.e., $\Omega \subset \mathbb{R}^D$) describes the support on which the GP approximations are valid (see also [Solin and Särkkä, 2020](#), for details). Crucially, these eigenvalues and eigenfunctions do not depend on the specific choice of the kernel or its hyperparameters—only the spectral density \mathcal{S}_i does.

Following [Riutort-Mayol et al. \(2023\)](#), the kernels can then be approximated using a set of M basis functions:⁸

$$g_i(\mathbf{f}_t) \approx \sum_{m=1}^M \phi_m(\mathbf{f}_t) c_{im}, \quad c_{im} \sim \mathcal{N}\left(0, \mathcal{S}_i(\sqrt{\boldsymbol{\lambda}_m})\right). \quad (7)$$

These approximations, for $i = 1, \dots, N$, allow us to rewrite Eq. (1) as:

$$\mathbf{y}_t = \mathbf{C}\boldsymbol{\Phi}(\mathbf{f}_t) + \mathbf{v}_t, \quad (8)$$

with the $N \times M$ -matrix \mathbf{C} comprising the weights c_{im} across equations $i = 1, \dots, N$, and basis functions $m = 1, \dots, M$, and the basis functions are stored in an $M \times 1$ -vector $\boldsymbol{\Phi}(\mathbf{f}_t) = (\phi_1(\mathbf{f}_t), \dots, \phi_M(\mathbf{f}_t))'$. Note that the derivations above are applicable to any generic stationary kernel. Next, we focus on distinct aspects that arise for the multiplicative and additive variants that we mentioned earlier. Indeed, the two squared exponential covariance functions in Eq. (4) are both stationary and therefore the associated spectral

⁸ The covariance function within Ω with inputs $\mathbf{f}_t, \mathbf{f}_\tau \in \Omega$ may be written as $\mathcal{K}_i(\mathbf{f}_t, \mathbf{f}_\tau) = \sum_{m=1}^{\infty} \mathcal{S}_i(\sqrt{\boldsymbol{\lambda}_m}) \phi_m(\mathbf{f}_t) \phi_m(\mathbf{f}_\tau)$. We may truncate this sum so that it can be used to obtain the weight space representation of the GP in Eq. (7).

densities are Fourier duals:

$$\mathcal{S}_i(\boldsymbol{\omega}) = \begin{cases} \xi_i(2\pi)^{D/2} \left(\prod_{j=1}^D \ell_{ij} \right) \cdot \exp \left(-\frac{1}{2} \sum_{j=1}^D \ell_{ij}^2 \omega_j^2 \right), & \text{for } \mathcal{K}_{i,\mathbf{M}}, \\ \xi_i(2D^2\pi)^{1/2} \left(\sum_{j=1}^D \ell_{ij} \cdot \exp \left(-\frac{1}{2} \ell_{ij}^2 \omega_j^2 \right) \right), & \text{for } \mathcal{K}_{i,\mathbf{A}}, \end{cases}$$

with a vector $\boldsymbol{\omega} = (\omega_1, \dots, \omega_D)'$ in the frequency domain.

Multiplicative squared exponential kernel. Let $\mathbb{S} \in \mathbb{R}^{M \times D}$ be the matrix of all possible combinations of univariate eigenfunctions across dimensions (i.e., all D -tuples), and we obtain for $m = 1, \dots, M$:

$$\boldsymbol{\lambda}_m = \left(\left\{ \frac{(\pi \mathbb{S}_{mj})^2}{4L^2} \right\}_{j=1}^D \right)', \quad \phi_m(\mathbf{f}_t) = \prod_{j=1}^D L^{-1/2} \sin \left(\lambda_{\mathbb{S}_{mj}}^{1/2} (f_{jt} + L) \right).$$

With a D -dimensional input space, the total number of eigenvalues and eigenfunctions used for the approximation is equal to the number of possible combinations of univariate eigenfunctions across all dimensions, i.e., $M = \tilde{M}^D$ where \tilde{M} is the number of basis functions for each dimension. In case of the multiplicative squared exponential kernel, the approximation changes the computational complexity to $\mathcal{O}((T+1)M^D)$ from $\mathcal{O}(T^3)$, a significant saving as long as the number of factors remains low.

Additive squared exponential kernel. Large macroeconomic datasets often require a moderate number of factors to fit the data. For example, [McCracken and Ng \(2021\)](#) find seven or eight factors in the full FRED-QD dataset, which would be rather computationally demanding when used with the multiplicative squared exponential kernel. For this reason, we introduce the additive squared exponential kernel as a more computationally efficient alternative.

Start by noting that the GP with this kernel is $g_i(\mathbf{f}_t) \sim \mathcal{GP}(0, \sum_{j=1}^D \mathcal{K}_i(f_{jt}, f_{jt}))$, which can be split into the sum of D univariate GPs, $y_{it} = g_i(f_{1t}) + \dots + g_i(f_{Dt}) + v_{it}$. Let \tilde{M} now denote the number of basis functions for each dimension ($j = 1, \dots, D$). Then the total number of eigenvalues/eigenfunctions used for the approximation is equal to $M = \tilde{M}^D$ for the multiplicative kernel, while it is $M = D \times \tilde{M}$ for the additive kernel.

This is because we can consider $\mathbb{S} \in \mathbb{R}^{\tilde{M}}$ for each dimension separately and simply sum over the factor-specific basis functions given the additive structure:

$$\boldsymbol{\lambda}_{mj} = \left(\left\{ \frac{(\pi \mathbb{S}_{mj})^2}{4L^2} \right\}_{j=1}^D \right)', \quad \phi_m(\mathbf{f}_t) = \sum_{j=1}^D L^{-1/2} \sin \left(\lambda_{\mathbb{S}_{mj}}^{1/2} (f_{jt} + L) \right).$$

This seems to be a classic trade-off between model flexibility and computational feasibility. The main limitations of the additive kernel variant is that it ignores interactions between latent factors, potentially underfitting highly complex relationships. On the other hand, it comes with the benefit of substantially improved scalability in the number of latent factors (D). One of the empirical contributions of our paper is investigating this trade-off in macroeconomic data.

2.4. Prior setup

As we adopt a fully Bayesian approach, we need to assign prior distributions to all unknown parameters in the model. For the measurement equation, we closely follow recent developments in the Gaussian process literature (see [van der Vaart and van Zanten, 2008](#); [Bhattacharya *et al.*, 2014](#); [Lindsten *et al.*, 2014](#); [Hauzenberger *et al.*, 2025](#)). Specifically, for the equation-specific (homoskedastic) measurement errors in Eq. (1), we assume independent inverse Gamma priors, $r_i \sim \mathcal{G}^{-1}(\nu_r, S_r)$, with $\nu_r = 3$ and $S_r = 0.3$ for all $i = 1, \dots, N$ equations. For the hyperparameters of the Gaussian processes kernels, we use Gamma priors on the unconditional variances, $\xi_i \sim \mathcal{G}(\nu_\xi, S_\xi)$, and Gamma priors on the inverse length-scale parameters, $\ell_{ij}^{-2} \sim \mathcal{G}(\nu_\ell, S_\ell)$. In the empirical application, We set $\nu_\xi = \nu_\ell = 0.5$ and $S_\xi = S_\ell = 0.5$, which is a weakly informative choice.

To specify priors for the parameters in the state equation, Eq. (2), we follow the recent macroeconomic DFM/VAR literature and adopt global–local shrinkage priors where appropriate (see, e.g., [Huber and Feldkircher, 2019](#); [Kaufmann and Schumacher, 2019](#); [Frühwirth-Schnatter *et al.*, 2025](#)). Specifically, we use horseshoe (HS, [Carvalho *et al.*, 2010](#)) priors, as they have been shown to work well in diverse contexts virtually free of tuning. Any hyperparameters associated with these priors are updated in a data-driven

manner, making the approach suitable for VARs of any size and providing a highly adaptive prior specification in the state equation. We defer technical details on the prior setup for the state equation to Section A.1 of the Appendix.

2.5. A Particle Gibbs sampling algorithm

To sample from the joint posterior distribution of our nonlinear state space model we rely on a Particle Gibbs approach. This section sketches the main steps of the algorithm, and additional details are provided in Section A.2 of the Appendix. Our Markov Chain Monte Carlo (MCMC) involves three main steps/blocks:

1. **Sample common latent factors.** We use Particle Gibbs with Ancestor Sampling (PGAS) to update $\{\mathbf{f}_t\}_{t=1}^T$ from its conditional posterior distribution (Andrieu *et al.*, 2010; Lindsten *et al.*, 2014). Andrieu *et al.* (2010) show how a version conditioning on a fixed trajectory for one of the particles can be used to produce draws that result in a Markov kernel with a target distribution that is invariant. However, the usual problem of path degeneracy in particle filters can result in poor mixing in the original version of this approach (especially for earlier periods in the sample). Recent development suggest that small modifications of this baseline algorithm can largely alleviate this problem.

In particular, Lindsten *et al.* (2014) propose the addition of a step that involves sampling the “ancestors” or indices associated with the particle that is being conditioned on. They show that this results in a substantial improvement in the mixing of the algorithm even with only a few particles. As explained in Lindsten *et al.* (2014), ancestor sampling breaks the reference path into segments allowing the particle system to collapse onto a new higher probability path. In the absence of ancestor sampling the particle system tends to collapse to the reference path; PGAS is outlined in detail in the first sampling block of Section A.2 in the Appendix.

2. **Sample unknown parameters in the measurement equation.** Most parameters can be sampled on an equation-by-equation basis (i.e., independently over $i = 1, \dots, N$)

using well-known conditional posterior distributions. The exception are the GP hyperparameters, which require equation-specific Metropolis-Hastings (MH) steps. We update:

- (i) **Variance of the idiosyncratic components r_i** : Using a conditionally conjugate inverse Gamma prior results in an inverse Gamma conditional posterior.
- (ii) **Coefficients in the observation equation $\mathbf{c}_i = (c_{i1}, \dots, c_{iM})'$** : As shown in Svensson *et al.* (2016), the reduced form approximation outlined in Section 2.3 implies a specific form for the conditional posterior of the coefficients in the observation equation. The conditional posterior is a multivariate Gaussian.
- (iii) **Kernel parameters $\boldsymbol{\theta}_i$** : To draw $\boldsymbol{\theta}_i$, we use an MH step with a random walk proposal. This amounts to proposing a candidate from suitable proposal, and computing the usual acceptance probability.

Specifics about these conditional posterior distributions and any associated moments are provided in the second block of Section A.2 in the Appendix.

3. Sample unknown parameters in the state equation. Conditional on a full history of \mathbf{f}_t , we sample the parameter in the state equation using the algorithm proposed in Carriero *et al.* (2022). These sampling steps for the state equation are outlined in detail in the third block of Section A.2 in the Appendix.

Typically none of the individual parameters of multivariate time series models are of primary interest, but functions of them are. In terms of computing forecasts and IRFs with the GP-DFM model, it suffices to note that the procedure is relatively straightforward. For the latent factors, we can iteratively project them τ steps ahead, $\mathbf{f}_{t+1}, \dots, \mathbf{f}_{t+\tau}$, using conventional tools for the linear VAR in the state equation (2). Once the path of the latent factors is known, we can use the approximated GP measurement equation (8) to obtain forecasts/IRFs for the endogenous variables.

3. FORECASTING THE US MACROECONOMY

In a first application, we assess the overall performance of the GP-DFM in an extensive forecasting exercise using data for the US macroeconomy. We use the popular FRED-QD dataset (see [McCracken and Ng, 2021](#)) which is a large information set spanning a broad array of quarterly macroeconomic data. Our evaluation sample is long enough to include several US macroeconomic events of importance: the dot-com bubble, the great financial crisis (GFC), and the COVID pandemic. We benchmark our main model specifications against a standard linear DFM which is a workhorse model in policy institutions for forecasting ([Giannone *et al.*, 2008](#); [Chernis and Sekkel, 2017](#)). Section 3.1 provides details on the forecasting setup as well as the competing specifications and Section 3.2 summarizes the main forecasting results.

3.1. Forecasting setup and competing specifications

The FRED-QD dataset covers 248 quarterly time series of which we select $N = 105$ to replicate the information content of [Stock and Watson \(2012\)](#). This rich macroeconomic dataset covers real activity, price, and financial variables. All variables are transformed to stationarity as suggested in [McCracken and Ng \(2021\)](#). For a list of variables used and transformations applied, see Appendix B. We define real output (GDPC1), non-farm employment (PAYEMS), consumer prices (CPIAUCSL) and the Federal funds rate (FEDFUNDS) as target variables for the forecasting exercise. We use an expanding window estimation scheme. The estimation sample starts in 1965Q1 and is recursively updated each quarter over the hold-out sample which spans 1992Q1 to 2023Q4. We consider forecast horizons of one-quarter, one-year and two-years ahead. For our target variables, we assess both joint and marginal density forecast accuracy. We use the energy score (ES) to evaluate the joint predictive densities and the continuous rank probability score (CRPS) to evaluate the marginal predictive densities ([Gneiting and Raftery, 2007](#)).

In the forecasting exercise, we consider 16 different model specifications, which vary across key modeling choices. For all models we use $P = 4$ lags in the state equation. The

margins we explore are linearity versus nonlinearity (or kernel choice) of the DFM: **linear DFM** for the linear specification, **GPDFM-A** for the GP-DFM with an additive kernel, and **GPDFM-M** for the GP-DFM with a multiplicative kernel. Moreover, we vary the number of factors ($D = \{2, 4, 8\}$) and consider either homoskedastic variances or SV of the state innovations. The out-of-sample forecasting exercise is used to assess all of these choices because it is robust and we do not have clear theoretical guidance for them. Finally, we need to decide on a few GP-DFM specific choices. For the multiplicative kernel, we set $\tilde{M} = 8$ for $D = 2$ and $\tilde{M} = 4$ for $D = 4$, and we do not consider $D = 8$.⁹ For the additive kernel, we set $\tilde{M} = 8$ for all values of D . The boundary condition L is specified in a semi-automatic manner as 1.2 times the maximum absolute value of the first D PCs.¹⁰

3.2. Out-of-sample forecasting evidence

Summary of findings. Before zooming into the details we provide a broad overview of the forecasting results. There are four main take aways. First, overall, the nonlinear DFM specifications consistently perform well and outperform the linear DFM, providing some improvements over the linear benchmark when considering both joint and marginal forecast losses. Second, the computationally efficient additive kernel method performs similarly to the more flexible multiplicative kernel, indicating that there is little trade-off between computation speed and forecast accuracy. Third, using only a relatively small number of factors is sufficient to forecast our target variables accurately. Forth, as is common in the macroeconomic literature, allowing for SV improves forecast accuracy.

In the following, Figs. 1 to 3 in this section report forecast evaluation metrics for both the joint forecast performance and the marginal forecast performances. For ease of readability, all figures follow a common convention. The benchmark model is a linear DFM with $D = 4$ and SV, and its absolute forecast score is reported directly. For other model

⁹ For the multiplicative kernel, $D = 8$ would result in a total of $M = \tilde{M}^8$ basis functions. Thus, setting $\tilde{M} = 4$ yields $M = 65536$, which is computationally burdensome.

¹⁰We have empirically tested different \tilde{M} values and our choices seem to be sensible ones in terms of the accuracy of the GP approximation.

specifications, we show the ratio relative to the benchmark. Ratios below one indicate superior performance relative to the benchmark (indicated by green-shaded cells), while ratios above one indicate inferior performance (indicated by red-shaded cells). Statistical significance is assessed using a one-sided Diebold and Mariano (1995) test, with asterisks denoting the significance of gains relative to the benchmark at the 1% (***), 5% (**), and 10% (*) level. For each horizon, the best performing specification is highlighted in bold.

Joint forecast performance over different evaluation periods. Figure 1 shows the joint forecast performance across horizons for three different evaluation samples. In panel (a) we consider the full evaluation sample, in panel (b) we stop prior to the COVID period in 2019Q4, and in panel (c) we stop prior to the GFC in 2007Q4. This strategy should help identify forecast gains over time. Recall our target variables are real output (GDPC1), non-farm payroll employment (PAYEMS), consumer prices (CPIAUCSL) and the Federal funds rate (FEDFUNDS); the losses in this context are based on the joint predictive distribution of these variables.

We first focus on panel (a) in Fig. 1, which shows the joint forecast performance for the full evaluation sample and serves as the main measure of model performance. As suggested in the key summarized findings mentioned above, we find that a GP-DFM variant with two factors and SV in the state equation consistently outperforms all other specifications across horizons. This model variant exhibits significant forecast improvements around 6 to 14% lower losses (as indicated by the dark green shaded cells).

When we vary the evaluation sample, we observe significant differences in the relative forecast performance of the GP-DFMs. Comparing panels (a) and (b) of Fig. 1 shows that including the COVID period systematically lowers ES ratios for our GP variants relative to the benchmark (but also relative to other linear competitors). This suggests that the impressive performance is partly driven by the period of the pandemic, and indicates that a flexible, nonlinear GP-DFM improves forecast accuracy over a more restrictive linear DFM during this exceptional period. Moreover, the improvements of the GP-DFM variants are largest at shorter horizons, outperforming linear competitors by larger margins. The best performing model improves upon the benchmark by nearly

14% for the full evaluation sample (and around 9% for the pre-COVID sample) at the one-quarter ahead horizon, while the improvement for the two-year ahead horizon is about 6%, irrespective of whether the evaluation stops before COVID.

Comparing panels (b) and (c) of Fig. 1, it is evident that the gains arise at least partially in the context of the GFC and the zero lower bound (ZLB). Indeed, the shorter (pre-GFC) period can be considered a relatively calmer economic period, and while there are some improvements for GP-DFM variants for the one-quarter and one-year horizon, the linear DFM benchmark is only occasionally outperformed, and typically not significantly so. For the two-year ahead horizon, however, the nonlinear model is more accurate, with significantly lower losses.

Marginal forecast performance. Figures 2 and 3 show the marginal forecast performance for the four target variables for different subsamples and across several forecast horizons. For one-quarter ahead forecasts we specifically look at the performance pre-GFC and the full sample. We do so because particularly at this horizon, GP-DFM shows sizable differences in joint relative performance, and the marginal perspective allows to investigate the sources of this accuracy premium also in terms of the cross-section of variables. For higher-order forecast horizons, we report the marginal scores only for the full evaluation sample in the interest of saving space.

Focusing first on the results at the one-quarter ahead horizon in Fig. 2, the CRPS ratios echo joint forecast performance patterns, and show that accuracy varies substantially across evaluation samples. Models with SV and a low number of factors perform particularly strongly for the full sample. All GP-DFM variants significantly outperform the linear benchmark at a 1% significance level (as well as the other linear competitors) for the Federal funds rate (FEDFUNDS). Here, the best performing specification, a GP-DFM with two factors, a multiplicative kernel, and SV, outperforms the benchmark by almost 14%. This is likely responsible for a sizable portion of the joint forecast performance. But this is not the sole source of the larger forecast accuracy gains for the full evaluation sample, as the GP-DFM also forecasts real output and inflation well. For real output (GDPC1), the best performing model is a GP-DFM equipped with two factors, an additive

Fig. 1: Joint forecast performance.

(a) Full evaluation sample from 1992Q1 to 2023Q4

		One-quarter ahead			One-year ahead			Two-year ahead		
homosk.	GPDFM-M	0.912**	0.892**		0.941	0.920*		0.959**	0.953***	
	GPDFM-A	0.892**	0.899**	0.895**	0.922*	0.921*	0.921*	0.968**	0.965***	0.964***
	linear DFM	1.028	1.049	1.069	1.024	1.032	1.038	1.014	1.002	1.024
SV	GPDFM-M	0.864***	0.877**		0.912**	0.907**		0.940***	0.942***	
	GPDFM-A	0.871***	0.871***	0.878***	0.907**	0.910**	0.915*	0.949***	0.949***	0.957***
	linear DFM	1.017	0.331	1.052	1.022	0.338	1.047	1.048	0.329	1.023
		2	4	8	2	4	8	2	4	8
		D								

(b) Pre-COVID evaluation sample from 1992Q1 to 2019Q4

		One-quarter ahead			One-year ahead			Two-year ahead		
homosk.	GPDFM-M	0.956	0.944		0.958	0.945		0.970**	0.960***	
	GPDFM-A	0.956	0.943	0.942	0.952	0.944	0.945	0.966**	0.969***	0.969***
	linear DFM	0.992	1.007	1.076	0.994	0.993	1.045	1.002	1.005	1.032
SV	GPDFM-M	0.913**	0.927*		0.930*	0.930*		0.938***	0.948***	
	GPDFM-A	0.920*	0.922**	0.923*	0.923*	0.931*	0.935	0.939***	0.943***	0.956***
	linear DFM	0.977*	0.299	1.052	0.977*	0.316	1.027	0.982**	0.317	1.023
		2	4	8	2	4	8	2	4	8
		D								

(c) Pre-GFC evaluation sample from 1992Q1 to 2007Q4

		One-quarter ahead			One-year ahead			Two-year ahead		
homosk.	GPDFM-M	1.027	1.021		1.004	0.998		0.974**	0.968***	
	GPDFM-A	1.026	1.016	1.023	0.995	0.991	0.999	0.968***	0.974***	0.975***
	linear DFM	0.980	1.005	1.047	1.006	1.018	1.060	1.000	1.008	1.036
SV	GPDFM-M	0.990	1.003		0.984	0.987		0.953**	0.963***	
	GPDFM-A	1.004	0.999	1.010	0.975	0.988	0.992	0.952***	0.955***	0.969***
	linear DFM	0.957**	0.293	1.019	0.984	0.325	1.042	0.981	0.341	1.018
		2	4	8	2	4	8	2	4	8
		D								

Notes: Energy scores (ES, [Gneiting and Raftery, 2007](#)) are used as a measure of joint forecast performance across all target variables. The gray-shaded entries refer to the absolute ES scores of a linear DFM with $D = 4$ and SV, which serves as the benchmark. A ratio smaller than one implies that the respective model outperforms the benchmark (indicated by a green-shaded cell), while a ratio greater than one implies that the respective model is outperformed by the benchmark (indicated by a red-shaded cell). Asterisks indicate statistical significance of forecast accuracy gains relative to the benchmark at the 1% (***), 5% (**), and 10% (*) significance levels, using a one-sided [Diebold and Mariano \(1995\)](#) test. The best performing specification for each horizon is in bold.

kernel, and homoskedastic errors, improving about 7% upon the benchmark (but these improvements are not statistically significant). For inflation (CPIAUCSL), most GP-DFM variants significantly outperform the benchmark at the 5% significance level, showing forecast performance similar to the best performing specification (in this case, a linear DFM with eight factors and SV). By contrast, for payroll employment (PAYEMS), there are no improvements.

Turning to the pre-GFC evaluation sample in panel (b), a linear DFM equipped with SV appears highly competitive and is difficult to outperform using GPs during this period (which largely coincides with the comparatively calm Great Moderation). Indeed, for the pre-GFC evaluation sample, virtually all GP-DFM variants perform similarly as the linear benchmark for GDPC1, CPIACUSL, and FEDFUNDS. However, the proposed nonlinear models struggle with forecasting PAYEMS at short horizons, even more so in “normal” economic times.

Moving to the one-year and two-year ahead horizons in Fig. 3, we see that a GP-DFM variant is consistently the best performing model across all variables. Specifically, the GP-DFM with SV and two factors performs very well. While we observe strong performance for the Federal funds rate similar to the short horizon, forecast performance for real activity variables generally improves at the longer horizons. In addition, inflation forecasts are better by a small but statistically significant amount (at the 5% significance level). The comparatively poor performance for short horizon forecasts of payroll employment also vanishes, with GP-DFM exhibiting more accurate forecasts than the benchmark (although these are not statistically significantly better).

Properties of real output growth forecast densities. In the final part of this section, we showcase the features of the predictive densities of a GP-DFM variant using real output growth around the COVID pandemic as a means to detect outliers and non-linearities. We can highlight what drives differences in forecast performance by comparing the predictive densities of the benchmark model against a GP-DFM variant.

Figure 4 shows the difference between the predictive densities of a GP-DFM variant with four factors, an additive kernel, and SV versus the linear DFM with four factors and

Fig. 2: Marginal one-quarter ahead forecast performance.

(a) Full evaluation sample from 1992Q1 to 2023Q4

		GDPC1			PAYEMS			CPIAUCSL			FEDFUNDS		
homosk.	GPDM-M	0.960	0.950		1.117	1.064		0.951**	0.953**		0.911**	0.892**	
	GPDM-A	0.932	0.942	0.942	1.049	1.037	1.074	0.956*	0.956**	0.956*	0.891**	0.899**	0.894**
	linear DFM	1.247	1.113	1.079	1.456	1.311	1.167	1.044	1.017	0.980	1.028	1.048	1.069
		2	4	8	2	4	8	2	4	8	2	4	8
SV	GPDM-M	0.950	0.942		1.023	1.041		0.950**	0.953**		0.864***	0.877***	
	GPDM-A	0.945	0.960	0.943	1.029	1.093	1.083	0.953**	0.955**	0.956*	0.870***	0.871***	0.877***
	linear DFM	1.064	0.005	1.025	1.072	0.003	1.064	1.009	0.003	0.947**	1.017	0.329	1.052
		2	4	8	2	4	8	2	4	8	2	4	8

(b) Pre-GFC evaluation sample from 1992Q1 to 2007Q4

		GDPC1			PAYEMS			CPIAUCSL			FEDFUNDS		
homosk.	GPDM-M	1.027	1.027		1.455	1.392		0.980	0.982		1.027	1.021	
	GPDM-A	1.023	1.021	1.027	1.376	1.384	1.443	0.980	0.984	0.988	1.026	1.016	1.023
	linear DFM	1.053	1.028	1.006	1.229	1.068	1.003	1.000	1.011	0.976*	0.980	1.005	1.047
		2	4	8	2	4	8	2	4	8	2	4	8
SV	GPDM-M	1.008	1.010		1.139	1.298		0.977*	0.988		0.990	1.003	
	GPDM-A	0.997	1.012	1.008	1.195	1.274	1.382	0.980	0.986	0.981	1.004	0.999	1.010
	linear DFM	1.002	0.003	0.983	1.081	0.001	0.964**	0.995	0.002	0.964**	0.957**	0.292	1.019
		2	4	8	2	4	8	2	4	8	2	4	8

Notes: Continuous rank probability score (CRPS, [Gneiting and Raftery, 2007](#)) are used as a measure of marginal forecast performance for each target variable. The gray-shaded entries refer to the absolute CRPS scores of a linear DFM with $D = 4$ and SV, which serves as the benchmark. A ratio smaller than one implies that the respective model outperforms the benchmark (indicated by a green-shaded cell), while a ratio greater than one implies that the respective model is outperformed by the benchmark (indicated by a red-shaded cell). Asterisks indicate statistical significance of forecast accuracy gains relative to the benchmark at the 1% (***), 5% (**), and 10% (*) significance levels, using a one-sided [Diebold and Mariano \(1995\)](#) test. The best performing specification for each horizon is in bold.

SV.¹¹ To ensure a fair comparison, we focus on the same number of factors and allow both models to feature SV. By inspecting this figure, we can see that the GP-DFM predictive densities place more mass around the realized outcomes, while the linear DFM is more dispersed. This cannot be attributed to SV, which features in both models. Instead, the GP-DFM's tighter forecast densities are likely a key factor behind the improved forecast performance. Specifically, this is evident during the calmer post-COVID period (from 2021 to 2023) following the sharp downturn and rebound in output growth at the onset of the pandemic.

¹¹Such a comparison between predictive densities has been proposed in [Diebold et al. \(2023\)](#).

Fig. 3: Marginal higher-order forecast performance (full evaluation sample).

(a) One-year ahead

		GDPC1			PAYEMS			CPIAUCSL			FEDFUNDS		
homosk.	GPDFM-M	0.954	0.954		0.983	0.948		0.972**	0.967**		0.941	0.920*	
	GPDFM-A	0.940*	0.943*	0.944	0.968	0.944	0.951	0.966**	0.969**	0.970**	0.922*	0.921*	0.921*
	linear DFM	1.150	0.991	0.987	1.171	1.039	0.989	1.009	0.998	0.985	1.024	1.033	1.039
SV	GPDFM-M	0.944*	0.941*		0.923	0.931		0.974**	0.968**		0.912**	0.907**	
	GPDFM-A	0.942*	0.958*	0.947*	0.930	0.954	0.952	0.972**	0.975*	0.973*	0.907**	0.910**	0.915*
	linear DFM	1.083	0.005	1.012	1.101	0.004	1.009	0.991	0.003	1.003	1.022	0.336	1.047
		2	4	8	2	4	8	2	4	8	2	4	8

(b) Two-year ahead

		GDPC1			PAYEMS			CPIAUCSL			FEDFUNDS		
homosk.	GPDFM-M	0.946*	0.947*		0.933	0.934		0.981**	0.979**		0.959**	0.953***	
	GPDFM-A	0.949	0.942	0.946	0.947	0.928	0.929	0.977*	0.979**	0.978**	0.968**	0.966***	0.964***
	linear DFM	1.022	0.982	0.968	1.030	0.973	0.959	0.998	0.992	0.991	1.015	1.002	1.025
SV	GPDFM-M	0.945*	0.949		0.924	0.928		0.978**	0.977**		0.941***	0.942***	
	GPDFM-A	0.945*	0.947*	0.943*	0.929	0.933	0.929	0.975**	0.980**	0.984**	0.950***	0.949***	0.957***
	linear DFM	1.047	0.005	1.000	1.079	0.004	1.004	0.995	0.003	1.006	1.048	0.328	1.023
		2	4	8	2	4	8	2	4	8	2	4	8

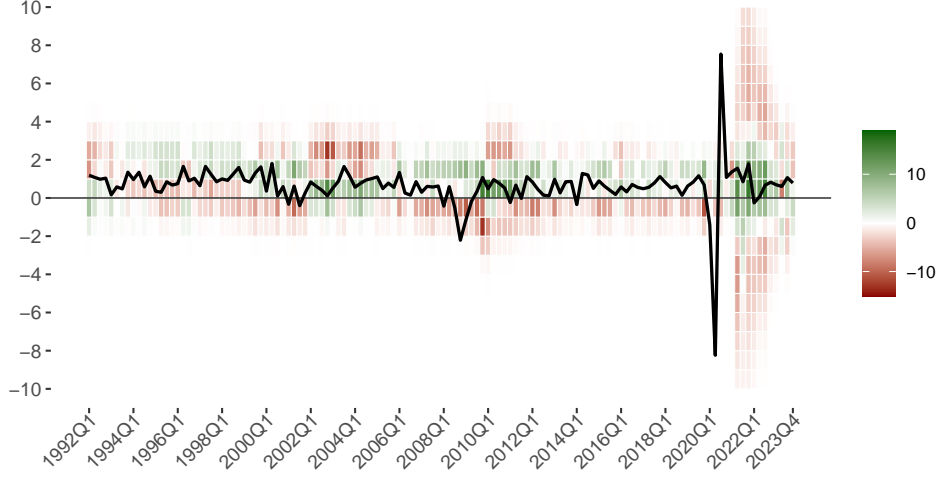
Notes: Continuous rank probability score (CRPS, Gneiting and Raftery, 2007) are used as a measure of marginal forecast performance for each target variable. The gray-shaded entries refer to the absolute CRPS scores of a linear DFM with $D = 4$ and SV, which serves as the benchmark. A ratio smaller than one implies that the respective model outperforms the benchmark (indicated by a green-shaded cell), while a ratio greater than one implies that the respective model is outperformed by the benchmark (indicated by a red-shaded cell). Asterisks indicate statistical significance of forecast accuracy gains relative to the benchmark at the 1% (***), 5% (**), and 10% (*) significance levels, using a one-sided Diebold and Mariano (1995) test. The best performing specification for each horizon is in bold.

4. DECOMPOSING THE DRIVERS OF GLOBAL INFLATION

Our second application demonstrates how to use the model for a semi-structural analysis, by investigating the importance of nonlinearities in macroeconomic data. Specifically, we explore the co-movement in cross-country consumer price index (CPI) inflation rates in the spirit of Mumtaz and Surico (2012) and Ha *et al.* (2023). We estimate the following model:

$$\pi_{it} = g_i(f_{W,t}) + s_i \cdot h_i(f_{D,t}) + (1 - s_i) \cdot h_i(f_{E,t}) + e_{it}. \quad (9)$$

Fig. 4: Assessment of one-year ahead real output growth predictive densities.



Notes: This figure shows the difference in predictive probabilities between the GP-DFM variant with four factors, an additive kernel, and SV, and the linear DFM with four factors and SV (see Diebold *et al.*, 2023). The grid ranges from -10% to 10% in increments of 1% . Green (red) shaded cells indicate that the GP-DFM increases (reduces) probability relative to the linear DFM in a certain region. The black solid line denotes the realized real output growth rate (GDPC1).

The panel of (quarterly) CPI inflation rates, π_{it} , is taken from the World Bank inflation database compiled by Ha *et al.* (2023), which runs from 1970Q1 to 2023Q4 and includes $N_D = 27$ developed countries as well as $N_E = 34$ emerging economies (EMDEs), such that $i = 1, 2, \dots, N_D, N_D + 1, \dots, N$, with $N = N_D + N_E$. Let $\mathbb{I}(\bullet)$ refer to an indicator function, and define $s_i = \mathbb{I}(i \leq N_D)$. That is, $s_i = 1$ if the respective country is among the developed countries and 0 when it is an emerging economy. Following Ha *et al.* (2023), inflation is decomposed into a global “world” factor (indicated with \mathbf{W}) that is common to all countries ($f_{\mathbf{W},t}$) and regional factors that are specific to country groups, namely developed countries ($f_{\mathbf{D},t}$) and EMDEs ($f_{\mathbf{E},t}$). As each inflation series might show a certain of idiosyncratic persistence, we assume that the idiosyncratic errors in the observation equation follow an AR(2) process: $e_{it} = \sum_{q=1}^2 \rho_{iq} e_{it-q} + v_{it}$, $v_{it} \sim N(0, r_i)$, which is a straightforward extension.

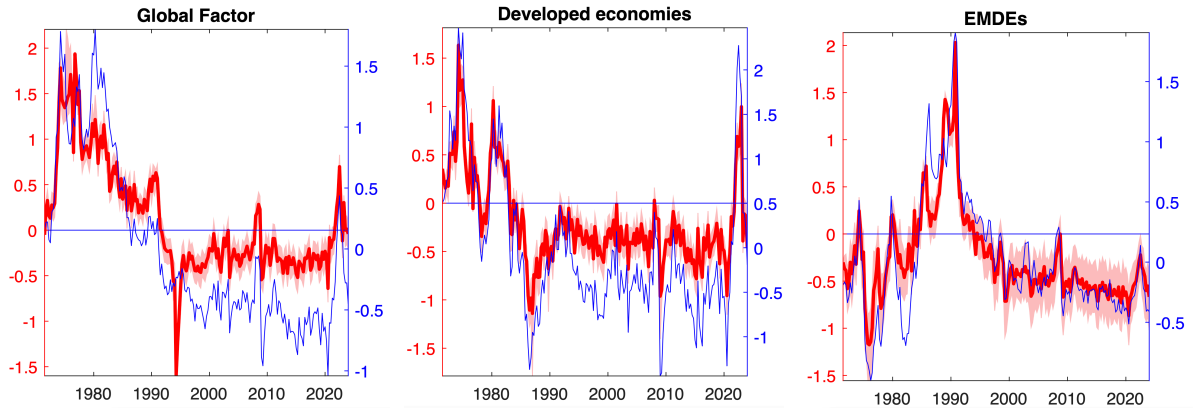
Unlike the previous literature, we allow the relationship between factors and observables to be nonlinear via the unknown functions $g_i(\bullet)$ and $h_i(\bullet)$. Our measurement equation allows for state-dependence and time-varying contributions from factors to observables. Note Eq. (9) corresponds to using an additive kernel similar to the previous

section, with $g_i(\bullet)$ specific to $f_{W,t}$ and $h_i(\bullet)$ specific to the relevant regional factor. We assume a GP with a squared exponential kernel for each function that are approximated using $\tilde{M} = 8$ basis functions. The regional factors are disentangled by imposing exclusion restrictions as in Eq. (9). That is, the regional factor for developed economies does not affect EMDEs and vice versa. We normalize the sign and scale of the factor by using a tight prior on the first row of loadings in each regional group.¹² The latent factors $\mathbf{f}_t = (f_{W,t}, f_{D,t}, f_{E,t})'$ are assumed to evolve according to a VAR(4) process, see Eq. (2), with $P = 4$.

4.1. Features of the GP-DFM inflation factors

Figure 5 plots the estimated posterior distribution of the three factors. The global factor has a distinct peaks in the earlier part of the sample in 1974Q1 correspond to the aftermath of the oil shock. After 1990, the global factor displays a declining trend consistent with the Great Moderation. This came to an end with a sharp rise in 2022Q1, possibly associated with supply disruptions in the post-COVID period.

Fig. 5: Estimated inflation factors of the GP-DFM.



Note: The figure displays the posterior estimates of the factors from the GP-DFM model. The red lines display the median estimates while the red shaded areas indicate the 68% confidence intervals. The blue lines represent the posterior medians of the factors from a linear DFM.

The factor specific to developing economies is persistently high during the mid-1970s and then during the early 1980s. The decline in this factor in 1985 precedes the fall

¹²The prior is obtained using an initial estimate of the weights obtained conditional on principal component estimate of the factors.

in global factor and is much sharper. In the subsequent period, inflation in developing countries appears to have been stable with the abrupt disruption after 2021. The variation in inflation specific to EMDEs appears radically different. The main peaks in the EMDE factor occurs in 1989 and 1990 capturing the aftermath of debt crises and hyperinflation in several countries.

It is interesting to note that while the estimated factors from the benchmark model are broadly similar to that obtained from the linear DFM, there are noticeable differences. For example, the global factor from the benchmark model has a smaller peak in 1980 when compared to the estimate from the linear DFM and displays sharper movements in 1994 and 2008. The developed country factor in the benchmark case displays less variation than the linear factor during the 1990s and 2000s while the EMDE factor has a smaller peak during the mid-1980s than the linear counterpart.

4.2. The importance of nonlinearities

This section investigates if there are meaningful nonlinearities between factors and observables. We study this by varying the size and sign of shock applied to the factors and compute generalized forecast error variance decompositions (GFEVD). A linear model would show no difference in the GFEVD for different size/sign shocks whereas if nonlinearities are important there would be substantial differences. For example, a large negative global inflation shock would have a proportionally different impact than a small positive shock in a nonlinear model.

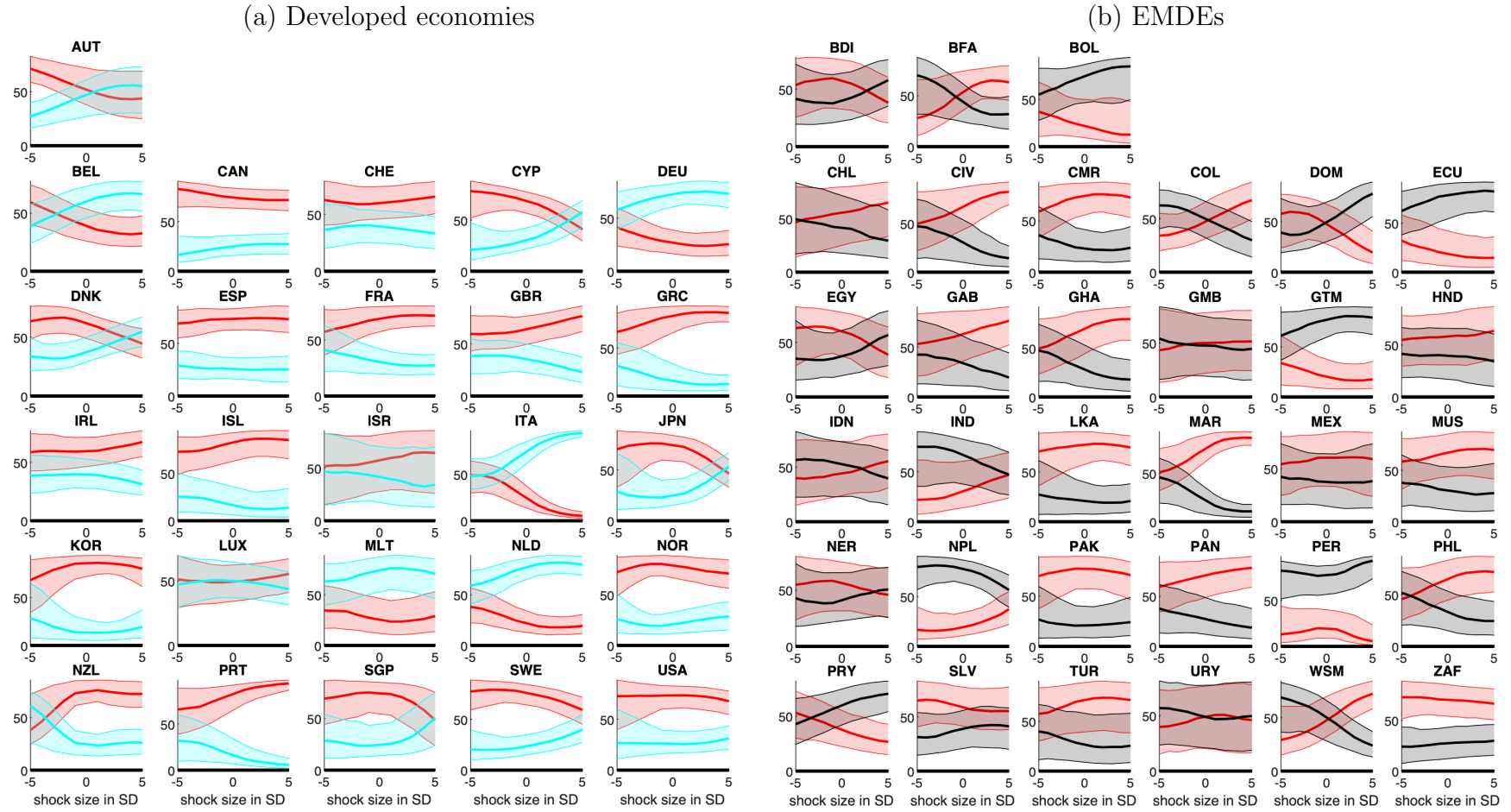
More specifically, we compute generalized impulse responses (GIRFs, [Koop *et al.*, 1996](#)), using a Cholesky decomposition of the reduced form covariance matrix to orthogonalize the structural disturbances (see also [Pfarrhofer and Stelzer, 2025](#), for related discussions). In the state equation VAR, we order the global factor first, followed by the developed economy and the EMDE factor, respectively. The GIRFs are calculated using the estimated factors in every fourth quarter of the sample as initial conditions. We use the generalised forecast error variance decomposition (GFEVD) to estimate the contribution

of the global and group specific factors to country-specific inflation rates. The GFEVD is calculated using the method proposed by [Lanne and Nyberg \(2016\)](#) whereby the GIRFs are used in the standard formula for the FEVD of a linear VAR model. This ensures that the decomposition adds up to one, while retaining properties such as dependence on initial conditions and on the size and sign of the shock being considered.

Panel (a) in [Fig. 6](#) shows that the contribution of the global and regional factors to the forecast error variance of inflation in developed countries. There is a clear dependence of the contributions on the sign and size of the shock. For example, the contribution of the world (regional) factor is lower (higher) for large positive shocks in Austria, Belgium, Cyprus, Denmark, Italy, Netherlands and Japan. The opposite result appears to hold for countries such as the UK, Greece, New Zealand, and Portugal.

Panel (b) [Figure 6](#) shows that for many EMDEs the importance of the world factor also depends on the size and sign of the shock. This is especially apparent for countries such as Burkina Faso, Colombia, Morocco and Ghana. For these countries, the regional factor contributes more to inflation fluctuations when shocks to this factor are negative.

Fig. 6: Forecast error variance decomposition of country-specific inflation series.



Note: The figure displays the contribution to the forecast error variance of inflation at the one-year horizon of shocks to the global factor (red), developed country factor (blue) for different shock sizes. The contributions are averaged across initial conditions. The solid lines are medians while the shaded areas represent the 68% confidence intervals.

5. CONCLUSIONS

In this paper we propose a class of nonlinear dynamic factor models using Gaussian Processes. Our first contribution is developing an estimation approach. Furthermore, we show that this model performs well and is easy to use for structural applications. The estimation algorithm we develop makes estimation of the GP-DFM feasible by addressing many of the drawbacks of Gaussian process models. For example, a GP models have difficulties scaling and filtering unobserved states in nonlinear models is difficult. We show how to solve these problems with an efficient estimation approach using Hilbert space approximations and particle sampling with ancestor sampling. Additionally, we show how to further increase computational speed using an additive kernel so that the model can handle moderate numbers of factors. Succinctly, we make using a nonlinear dynamic factor model feasible in macroeconomic applications.

We assess the GP-DFM in a forecasting exercise using US macroeconomic data. We show that the GP-DFM with SV outperforms linear versions of the model. Specifically, it performs well when there are nonlinearities in the data such as at the effective lower bound and during COVID. On average, its performance is driven by its more precise predictive densities. Finally, there is little cost for using an additive kernel, which excludes interactions between factors, suggesting that interaction terms are not an important type of nonlinearity in this dataset.

We also demonstrate how such a model could be used for a semi-structural analysis. We show that our specification with a nonlinear measurement equation and linear state equation makes for easy inference. The linear state equation allows us to apply structural VAR techniques to the factors while the nonlinear measurement equation allows for flexibility in how the factor maps to observables (state-dependence and time-variation). Our example investigates the co-movement in cross-country CPU inflation rates. First we find differences between the factors estimated in a linear DFM and a GP-DFM. Second, we investigate the importance of nonlinearities by examining how the size and sign of

shocks affect contributions to the forecast error variance decomposition. This shows the importance of allowing for nonlinearities.

REFERENCES

- ADRIAN T, BOYARCHENKO N, AND GIANNONE D (2019), “Vulnerable Growth,” *American Economic Review* **109**(4), 1263–1289.
- AGUILAR O, AND WEST M (2000), “Bayesian dynamic factor models and portfolio allocation,” *Journal of Business & Economic Statistics* **18**(3), 338–357.
- ANDREINI P, IZZO C, AND RICCO G (2023), “Deep Dynamic Factor Models,” *arXiv* 2007.11887.
- ANDRIEU C, DOUCET A, AND HOLENSTEIN R (2010), “Particle Markov chain Monte Carlo methods,” *Journal of the Royal Statistical Society Series B* **72**(3), 269–342.
- BABII A, GHYSELS E, AND STRIAUKAS J (2022), “Machine learning time series regressions with an application to nowcasting,” *Journal of Business & Economic Statistics* **40**(3), 1094–1106.
- BAI J, AND NG S (2008), “Forecasting economic time series using targeted predictors,” *Journal of Econometrics* **146**(2), 304–317.
- BALL LM, LEIGH D, AND MISHRA P (2022), “Understanding U.S. Inflation During the COVID Era,” Working Paper 30613, National Bureau of Economic Research.
- BAÑBURA M, GIANNONE D, AND REICHLIN L (2010), “Large Bayesian vector auto regressions,” *Journal of Applied Econometrics* **25**(1), 71–92.
- BASSETTI F, CASARIN R, AND LEISEN F (2014), “Beta-product dependent Pitman–Yor processes for Bayesian inference,” *Journal of Econometrics* **180**(1), 49–72.
- BEAUDRY P, HOU C, AND PORTIER F (2024), “The Dominant Role of Expectations and Broad-Based Supply Shocks in Driving Inflation,” Working Paper 32322, National Bureau of Economic Research.
- BENIGNO P, AND EGGERTSSON GB (2023), “It’s Baaack: The Surge in Inflation in the 2020s and the Return of the Non-Linear Phillips Curve,” Working Paper 31197, National Bureau of Economic Research.
- BHATTACHARYA A, PATI D, AND DUNSON D (2014), “Anisotropic function estimation using multi-bandwidth Gaussian processes,” *Annals of Statistics* **42**(1), 352.
- BOK B, CARATELLI D, GIANNONE D, SBORDONE AM, AND TAMBALOTTI A (2018), “Macroeconomic nowcasting and forecasting with big data,” *Annual Review of Economics* **10**(1), 615–643.
- BRUNNERMEIER MK, AND SANNIKOV Y (2014), “A Macroeconomic Model with a Financial Sector,” *American Economic Review* **104**(2), 379–421.
- CAMACHO M, PEREZ-QUIROS G, AND PONCELA P (2018), “Markov-switching dynamic factor models in real time,” *International Journal of Forecasting* **34**(4), 598–611.
- CARRIERO A, CHAN J, CLARK TE, AND MARCELLINO M (2022), “Corrigendum to ”Large Bayesian vector autoregressions with stochastic volatility and non-conjugate priors”[J. Econometrics 212 (1)(2019) 137–154],” *Journal of Econometrics* **227**(2), 506–512.
- CARTER CK, AND KOHN R (1994), “On Gibbs sampling for state space models,” *Biometrika* **81**(3), 541–553.
- CARVALHO CM, POLSON NG, AND SCOTT JG (2010), “The horseshoe estimator for sparse signals,” *Biometrika* 465–480.
- CHAN JC, AND JELIAZKOV I (2009), “Efficient simulation and integrated likelihood estimation in state space models,” *International Journal of Mathematical Modelling and Numerical Optimisation* **1**(1-2), 101–120.

- CHAUVET M (1998), “An Econometric Characterization of Business Cycle Dynamics with Factor Structure and Regime Switching,” *International Economic Review* **39**(4), 969–996.
- CHAUVET M, AND SENYUZ Z (2016), “A dynamic factor model of the yield curve components as a predictor of the economy,” *International Journal of Forecasting* **32**(2), 324–343.
- CHENG MY, AND WU HT (2013), “Local linear regression on manifolds and its geometric interpretation,” *Journal of the American Statistical Association* **108**(504), 1421–1434.
- CHERNIS T, AND SEKKEL R (2017), “A dynamic factor model for nowcasting Canadian GDP growth,” *Empirical Economics* **53**(1), 217–234.
- CHRONOPOULOS I, RAFTAPOSTOLOS A, AND KAPETANIOS G (2024), “Forecasting value-at-risk using deep neural network quantile regression,” *Journal of Financial Econometrics* **22**(3), 636–669.
- CLARK TE (2011), “Real-time density forecasts from Bayesian vector autoregressions with stochastic volatility,” *Journal of Business & Economic Statistics* **29**(3), 327–341.
- CLARK TE, HUBER F, AND KOOP G (2025), “A Nonparametric Approach to Augmenting a Bayesian VAR with Nonlinear Factors,” *arXiv* 2508.13972.
- CLARK TE, HUBER F, KOOP G, AND MARCELLINO M (2024a), “Forecasting US inflation using Bayesian nonparametric models,” *The Annals of Applied Statistics* **18**(2), 1421–1444.
- CLARK TE, HUBER F, KOOP G, MARCELLINO M, AND PFARRHOFER M (2024b), “Investigating growth-at-risk using a multicountry nonparametric quantile factor model,” *Journal of Business & Economic Statistics* **42**(4), 1302–1317.
- CLARK TE, AND RAVAZZOLO F (2015), “Macroeconomic forecasting performance under alternative specifications of time-varying volatility,” *Journal of Applied Econometrics* **30**(4), 551–575.
- COGLEY T, AND SARGENT TJ (2005), “Drifts and volatilities: monetary policies and outcomes in the post WWII US,” *Review of Economic Dynamics* **8**(2), 262–302.
- DEL NEGRO M, AND OTROK C (2008), “Dynamic factor models with time-varying parameters: measuring changes in international business cycles,” Staff Report 326, Federal Reserve Bank of New York.
- DIEBOLD FX, AND MARIANO RS (1995), “Comparing predictive accuracy,” *Journal of Business & Economic Statistics* **13**(3), 253–263.
- DIEBOLD FX, SHIN M, AND ZHANG B (2023), “On the aggregation of probability assessments: Regularized mixtures of predictive densities for Eurozone inflation and real interest rates,” *Journal of Econometrics* **237**(2, Part C), 105321.
- DOZ C, AND FULEKY P (2020), “Dynamic factor models,” *Macroeconomic Forecasting in the Era of Big Data: Theory and Practice* 27–64.
- FARRELL MH, LIANG T, AND MISRA S (2021), “Deep neural networks for estimation and inference,” *Econometrica* **89**(1), 181–213.
- FORNI M, HALLIN M, LIPPI M, AND REICHLIN L (2000), “The generalized dynamic-factor model: Identification and estimation,” *Review of Economics and statistics* **82**(4), 540–554.
- FRIGOLA R, LINDSTEN F, SCHÖN TB, AND RASMUSSEN CE (2013), “Bayesian Inference and Learning in Gaussian Process State-Space Models with Particle MCMC,” in C BURGESS, L BOTTOU, M WELLING, Z GHAHRAMANI, AND K WEINBERGER (eds.) “Advances in Neural Information Processing Systems,” volume 26, Curran Associates, Inc.
- FRÜHWIRTH-SCHNATTER S (1994), “Data augmentation and dynamic linear models,” *Journal of Time Series Analysis* **15**(2), 183–202.

- FRÜHWIRTH-SCHNATTER S, HOSSZEJNI D, AND LOPES HF (2025), “Sparse Bayesian factor analysis when the number of factors is unknown (with discussion),” *Bayesian Analysis* **20**(1), 213–344.
- GEWEKE J, AND AMISANO G (2010), “Comparing and evaluating Bayesian predictive distributions of asset returns,” *International Journal of Forecasting* **26**(2), 216–230.
- GIANNONE D, LENZA M, AND PRIMICERI GE (2021), “Economic predictions with big data: The illusion of sparsity,” *Econometrica* **89**(5), 2409–2437.
- GIANNONE D, REICHLIN L, AND SMALL D (2008), “Nowcasting: The real-time informational content of macroeconomic data,” *Journal of Monetary Economics* **55**(4), 665–676.
- GNEITING T, AND RAFTERY AE (2007), “Strictly proper scoring rules, prediction, and estimation,” *Journal of the American statistical Association* **102**(477), 359–378.
- GOULET COULOMBE P (2024), “The macroeconomy as a random forest,” *Journal of Applied Econometrics* **39**(3), 401–421.
- GOULET COULOMBE P, LEROUX M, STEVANOVIC D, AND SURPRENANT S (2022), “How is machine learning useful for macroeconomic forecasting?” *Journal of Applied Econometrics* **37**(5), 920–964.
- GUERRÓN-QUINTANA P, KHAZANOV A, AND ZHONG M (2023), “Financial and Macroeconomic Data Through the Lens of a Nonlinear Dynamic Factor Model,” *FEDS Working Paper* **2023-27**.
- HA J, KOSE MA, AND OHNSORGE F (2023), “One-stop source: A global database of inflation,” *Journal of International Money and Finance* **137**, 102896.
- HAMILTON JD (1989), “A new approach to the economic analysis of nonstationary time series and the business cycle,” *Econometrica* 357–384.
- (2001), “A parametric approach to flexible nonlinear inference,” *Econometrica* **69**(3), 537–573.
- HAUZENBERGER N, HUBER F, AND KLIEBER K (2023), “Real-time inflation forecasting using non-linear dimension reduction techniques,” *International Journal of Forecasting* **39**(2), 901–921.
- HAUZENBERGER N, HUBER F, KLIEBER K, AND MARCELLINO M (2024a), “Bayesian neural networks for macroeconomic analysis,” *Journal of Econometrics* 105843.
- HAUZENBERGER N, HUBER F, MARCELLINO M, AND PETZ N (2025), “Gaussian process vector autoregressions and macroeconomic uncertainty,” *Journal of Business & Economic Statistics* **43**(1), 27–43.
- HAUZENBERGER N, MARCELLINO M, PFARRHOFER M, AND STELZER A (2024b), “Bayesian Nowcasting with mixed frequency data using gaussian processes,” *arXiv* 2402.10574.
- HUBER F, AND FELDKIRCHER M (2019), “Adaptive shrinkage in Bayesian vector autoregressive models,” *Journal of Business & Economic Statistics* **37**(1), 27–39.
- HUBER F, KOOP G, ONORANTE L, PFARRHOFER M, AND SCHREINER J (2023), “Nowcasting in a pandemic using non-parametric mixed frequency VARs,” *Journal of Econometrics* **232**(1), 52–69.
- JIN X, MAHEU JM, AND YANG Q (2022), “Infinite Markov pooling of predictive distributions,” *Journal of Econometrics* **228**(2), 302–321.
- KALLI M, AND GRIFFIN JE (2018), “Bayesian nonparametric vector autoregressive models,” *Journal of Econometrics* **203**(2), 267–282.
- KASTNER G, AND FRÜHWIRTH-SCHNATTER S (2014), “Ancillarity-sufficiency interweaving strategy (ASIS) for boosting MCMC estimation of stochastic volatility models,” *Computational Statistics & Data Analysis* **76**, 408–423.
- KAUFMANN S, AND SCHUMACHER C (2019), “Bayesian estimation of sparse dynamic factor models with order-independent and ex-post mode identification,” *Journal of Econometrics* **210**(1), 116–134.

- KLIEBER K (2024), “Non-linear dimension reduction in factor-augmented vector autoregressions,” *Journal of Economic Dynamics and Control* **159**, 104800.
- KOOP G, AND KOROBILIS D (2013), “Large time-varying parameter VARs,” *Journal of Econometrics* **177**(2), 185–198.
- KOOP G, PESARAN MH, AND POTTER SM (1996), “Impulse response analysis in non-linear multivariate models,” *Journal of Econometrics* **74**(1), 119–147.
- KOROBILIS D (2013), “Assessing the transmission of monetary policy using time-varying parameter dynamic factor models,” *Oxford Bulletin of Economics and Statistics* **75**(2), 157–179.
- KOSE MA, OTROK C, AND WHITEMAN CH (2003), “International business cycles: World, region, and country-specific factors,” *American Economic Review* **93**(4), 1216–1239.
- LANNE M, AND NYBERG H (2016), “Generalized Forecast Error Variance Decomposition for Linear and Nonlinear Multivariate Models,” *Oxford Bulletin of Economics and Statistics* **78**(4), 595–603.
- LEE J, BAHRI Y, NOVAK R, SCHOENHOLZ SS, PENNINGTON J, AND SOHL-DICKSTEIN J (2018), “Deep Neural Networks as Gaussian Processes,” .
- LINDSTEN F, JORDAN MI, AND SCHÖN TB (2014), “Particle Gibbs with Ancestor Sampling,” *Journal of Machine Learning Research* **15**(63), 2145–2184.
- LUO Y, PAIGE B, AND GRIFFIN J (2025), “Time-varying Factor Augmented Vector Autoregression with Grouped Sparse Autoencoder,” *arXiv* 2503.04386.
- MAKALIC E, AND SCHMIDT DF (2015), “A simple sampler for the horseshoe estimator,” *IEEE Signal Processing Letters* **23**(1), 179–182.
- MARCELLINO M, AND PFARRHOFFER M (2024), “Bayesian nonparametric methods for macroeconomic forecasting,” in MP CLEMENTS, AND AB GALVÃO (eds.) “Handbook of Research Methods and Applications in Macroeconomic Forecasting,” chapter 5, 90–125, Cheltenham, UK/Northampton, USA: Edward Elgar Publishing.
- MCCRACKEN MW, AND NG S (2016), “FRED-MD: A monthly database for macroeconomic research,” *Journal of Business & Economic Statistics* **34**(4), 574–589.
- (2021), “FRED-QD: A Quarterly Database for Macroeconomic Research,” *Review* **103**(1), 1–44.
- MEDEIROS MC, VASCONCELOS GF, VEIGA Á, AND ZILBERMAN E (2021), “Forecasting inflation in a data-rich environment: the benefits of machine learning methods,” *Journal of Business & Economic Statistics* **39**(1), 98–119.
- MUMTAZ H, AND SURICO P (2012), “Evolving international inflation dynamics: world and country-specific factors,” *Journal of the European Economic Association* **10**(4), 716–734.
- NEAL RM (1996), *Priors for Infinite Networks*, 29–53, New York, NY: Springer New York.
- PFARRHOFFER M, AND STELZER A (2025), “Scenario analysis with multivariate Bayesian machine learning models,” *arXiv* **2502.08440**.
- PRIMICERI GE (2005), “Time varying structural vector autoregressions and monetary policy,” *The Review of Economic Studies* **72**(3), 821–852.
- RIUTORT-MAYOL G, BÜRKNER PC, ANDERSEN MR, SOLIN A, AND VEHTARI A (2023), “Practical Hilbert space approximate Bayesian Gaussian processes for probabilistic programming,” *Statistics and Computing* **33**(1), 17.
- SIMS CA, AND ZHA T (2006), “Were there regime switches in US monetary policy?” *American Economic Review* **96**(1), 54–81.
- SNELLMAN O (2024), “Non-Linear Dynamic Factor Analysis With a Transformer Network,” *SSRN* 5000165.
- SOLIN A, AND SÄRKKÄ S (2020), “Hilbert space methods for reduced-rank Gaussian process regression,” *Statistics and Computing* **30**(2), 419–446.

- STOCK J, AND WATSON M (2016), “Dynamic Factor Models, Factor-Augmented Vector Autoregressions, and Structural Vector Autoregressions in Macroeconomics,” in JB TAYLOR, AND H UHLIG (eds.) “Handbook of Macroeconomics,” *Handbook of Macroeconomics*, volume 2, chapter 0, 415–525, Elsevier.
- STOCK JH, AND WATSON MW (2002), “Macroeconomic forecasting using diffusion indexes,” *Journal of Business & Economic Statistics* **20**(2), 147–162.
- (2012), “Disentangling the Channels of the 2007-2009 Recession,” Technical report, National Bureau of Economic Research.
- SVENSSON A, SOLIN A, SÄRKKÄ S, AND SCHÖN T (2016), “Computationally efficient Bayesian learning of Gaussian process state space models,” in “Artificial Intelligence and Statistics,” 213–221, PMLR.
- TERÄSVIRTA T (1994), “Specification, estimation, and evaluation of smooth transition autoregressive models,” *Journal of the american Statistical association* **89**(425), 208–218.
- TURNER R, DEISENROTH M, AND RASMUSSEN C (2010), “State-Space Inference and Learning with Gaussian Processes,” in YW TEH, AND M TITTERINGTON (eds.) “Proceedings of the Thirteenth International Conference on Artificial Intelligence and Statistics,” *Proceedings of Machine Learning Research*, volume 9, 868–875, Chia Laguna Resort, Sardinia, Italy: PMLR.
- VAN DER VAART AW, AND VAN ZANTEN JH (2008), “Rates of contraction of posterior distributions based on Gaussian process priors,” *The Annals of Statistics* **36**(3), 1435 – 1463.
- VELASCO S (2024), *Let the Tree Decide: FABART A Non-Parametric Factor Model*, Phd thesis, Queen Mary University of London, chapter 3 of “Essays on methods to cast nonlinear unobserved components”.
- WILLIAMS CK, AND RASMUSSEN CE (2006), *Gaussian processes for machine learning*, volume 2, Cambridge, MA, USA: MIT Press.
- ZHOU X, NAKAJIMA J, AND WEST M (2014), “Bayesian forecasting and portfolio decisions using dynamic dependent sparse factor models,” *International Journal of Forecasting* **30**(4), 963–980.

Online Appendix: A Bayesian Gaussian Process Dynamic Factor Model

A. TECHNICAL APPENDIX

The technical appendix provides further details on the priors used in the state equation (2) and on well-known steps of the Particle within Gibbs sampling algorithm.

A.1. Shrinkage prior setup for the state equation

To specify the priors on the parameters the parameters in the state equation, Eq. (2), define $\mathbf{A} = (\mathbf{A}_1, \dots, \mathbf{A}_P)$ and decompose $\mathbf{Q} = \mathbf{\Psi}^{-1} \mathbf{\Sigma} (\mathbf{\Psi}^{-1})'$ via Cholesky, where $\mathbf{\Psi}^{-1}$ is a lower unit triangular matrix and $\mathbf{\Sigma} = \text{diag}(\sigma_1^2, \dots, \sigma_D^2)$.

Specifically, on the coefficients of the VAR in Eq. (2), we use a horseshoe (HS, [Carvalho *et al.*, 2010](#)) prior to regularize the individual parameters in \mathbf{A} . Let a_{dj} denote the $(d, j)^{\text{th}}$ element in \mathbf{A} and \mathbf{a}_d denote the d^{th} row in \mathbf{A} . This prior amounts to $a_{dj} \sim \mathcal{N}(0, \varpi_{j, \mathbf{a}_d}^2 \varphi_{\mathbf{a}_d}^2)$, where $\varpi_{j, \mathbf{a}_d}^2$ refers to a local shrinkage scaling associated with the $(d, j)^{\text{th}}$ element, and $\varphi_{\mathbf{a}_d}^2$ is a global (factor-specific) shrinkage parameter common to all elements in \mathbf{a}_d . Both hyperparameters are then specified to follow a Half-Cauchy distribution: $\varpi_{j, \mathbf{a}_d} \sim \mathcal{C}^+(0, 1)$ and $\varphi_{\mathbf{a}_d} \sim \mathcal{C}^+(0, 1)$. While the global shrinkage parameter typically pushes all elements in \mathbf{a}_d strongly towards zero, the local shrinkage scalings allow for element-specific adjustments in the degree of shrinkage. Since both hyperparameters are updated in a data-driven manner, this makes the horseshoe prior particularly powerful and attractive for any VAR setting (small or large), as it provides an adaptive, tuning-free prior specification.

We also use a HS prior on the contemporaneous relationships. For this, we recast the reduced form VAR in Eq. (2) into its structural form (see [Carriero *et al.*, 2022](#)): $\mathbf{\Psi} \boldsymbol{\varepsilon}_t = \tilde{\boldsymbol{\varepsilon}}_t$, $\tilde{\boldsymbol{\varepsilon}}_t \sim \mathcal{N}(\mathbf{0}_D, \mathbf{\Sigma})$, with $\boldsymbol{\varepsilon}_t = \mathbf{f}_t - \sum_{p=1}^P \mathbf{A}_p \mathbf{f}_{t-p}$. On the free elements in $\mathbf{\Psi}$ (the inverse of $\mathbf{\Psi}^{-1}$, which collects the structural contemporaneous relationships), we specify

$\psi_{dj} \sim \mathcal{N}(0, \varpi_{j,\psi_d}^2 \varphi^2)$, for $d \geq 2$ and $d > j$. Here, ψ_{dj} denotes the $(d, j)^{\text{th}}$ element in Ψ and ϖ_{j,ψ_d}^2 the associated local shrinkage scaling (with ψ_d indicating the d^{th} row of Ψ) and φ^2 a global scaling parameter common to all free elements in Ψ . Analogously to the VAR coefficients above, we define $\varpi_{j,\psi_d} \sim \mathcal{C}^+(0, 1)$ and $\varphi \sim \mathcal{C}^+(0, 1)$.

For the structural error variances in the state equation, we specify either inverse Gamma priors $\sigma_d^2 \sim \mathcal{G}^{-1}(\nu_\sigma, S_\sigma)$ or, when using a stochastic volatility (SV) specification, we assume that the log-volatilities follow an AR(1) process: $\log \sigma_{dt}^2 = \varsigma_{dt} = \mu_{\varsigma_d} + \rho_{\varsigma_d} \varsigma_{dt-1} + \eta_{\varsigma_d}$, with $\eta_{\varsigma_d} \sim \mathcal{N}(0, \sigma_{\varsigma_d}^2)$. The latter has been found to be important in macroeconomic applications. Therefore we consider this straightforward extension in our empirical application(s) as well. This modification does not alter the general structure of the model. The only change is that the constant Σ is replaced by a time-varying Σ_t , featuring a t sub-index. For the prior distributions of the SV parameters, we follow [Kastner and Frühwirth-Schnatter \(2014\)](#) and specify a weakly informative Gaussian prior on μ_{ς_d} , a Beta prior on the transformed autoregressive parameter $(\rho_{\varsigma_d} + 1)/2$ and a Gamma shrinkage prior on the state innovation variance $\sigma_{\varsigma_d}^2$, which is supposed to push the model towards homoskedasticity.¹

A.2. Posterior sampling via MCMC

In this Section we provide the full details on the three main steps/blocks of our Markov chain Monte Carlo (MCMC) algorithm.

1. **Sample common latent factors.** We use a Particle Gibbs with Ancestor Sampling (PGAS) to update $\{\mathbf{f}_t\}_{t=1}^T$ from its conditional posterior distribution ([Andrieu *et al.*, 2010](#); [Lindsten *et al.*, 2014](#)). [Andrieu *et al.* \(2010\)](#) show how a version of the particle filter, conditioned on a fixed trajectory for one of the particles can be used to produce draws that result in a Markov kernel with a target distribution that is invariant. However, the usual problem of path degeneracy in the particle filter can result in poor mixing in the original version of particle Gibbs sampler. Recent development suggest

¹ For details, see [Kastner and Frühwirth-Schnatter \(2014\)](#).

that small modifications of this algorithm can largely alleviate this problem. In particular, [Lindsten *et al.* \(2014\)](#) propose the addition of a step that involves sampling the “ancestors” or indices associated with the particle that is being conditioned on. They show that this results in a substantial improvement in the mixing of the algorithm even with few particles. As explained in [Lindsten *et al.* \(2014\)](#), ancestor sampling breaks the reference path into segments allowing the particle system to collapse onto a new higher probability path. In the absence of ancestor sampling the particle system tends to collapse to the reference path. Therefore, we use the following particle Gibbs with ancestor sampling step.

We outline our nonlinear state space model, which we aim to sample from, in Eqs. (8) and (2). Eq. (8) is the measurement equation after applying the reduced-rank approximation, and Eq. (2) is the state equation, which follows a VAR(P) process. In the following, the VAR(P) in Eq. (2) can be rewritten more compactly in its companion form:

$$\tilde{\mathbf{f}}_t = \mathbf{B}\tilde{\mathbf{f}}_{t-1} + \mathbf{e}_t, \mathbf{e}_t \sim \mathcal{N}(0, \tilde{\mathbf{Q}}).$$

Here, $\tilde{\mathbf{f}}_t = (\mathbf{f}'_t, \mathbf{f}'_{t-1}, \dots, \mathbf{f}'_{t-(P-1)})'$, \mathbf{B} denotes the VAR parameters, \mathbf{e}_t the errors, $\tilde{\mathbf{Q}}$ the variance-covariance matrix in companion form.

Let $\tilde{\mathbf{f}}_t^{(s-1)}$, for $t = 1, 2, \dots, T$, denote the fixed trajectory obtained in the previous draw of our Gibbs sampler, corresponding to the $(s-1)^{\text{th}}$ iteration. Collect all the remaining parameters in the Θ and denote the number of particles by H . To obtain the s^{th} draw, the conditional particle filter with ancestor sampling proceeds in the following steps.

For period $t = 1$, we have:

- (i) For particles $h = 1, 2, \dots, (H-1)$, draw $\tilde{\mathbf{f}}_1^{(h)} | \tilde{\mathbf{f}}_0^{(h)}, \Theta$ and set the H^{th} particle to the previously accepted draw, $\tilde{\mathbf{f}}_1^{(H)} = \tilde{\mathbf{f}}_1^{(s-1)}$.

- (ii) Compute the normalized weights $\zeta_1^{(h)} = \frac{\exp(\tilde{\zeta}_1^{(h)})}{\sum_{k=1}^H \exp(\tilde{\zeta}_1^{(k)})}$, where $\tilde{\zeta}_1^{(h)}$ denotes the conditional log-likelihood defined as:

$$\log \mathcal{L}(\tilde{\mathbf{f}}_1^{(h)}) = -\frac{1}{2} \log(2\pi) - \frac{1}{2} \log(\det \mathbf{R}) - \frac{1}{2} (\mathbf{v}_1^{(h)} \mathbf{R}^{-1} \mathbf{v}_1^{(h)})'.$$

Here, $\mathbf{v}_1^{(h)}$ is computed by simply rearranging the measurement equation in Eq. (8) and plugging in $\mathbf{f}_1^{(h)}$: $\mathbf{v}_1^{(h)} = \mathbf{y}_1 - \mathbf{C}\Phi(\mathbf{f}_1^{(h)})$.

For the subsequent periods $t = 2, \dots, T$ we have:

- (i) Resample $\tilde{\mathbf{f}}_{t-1}^{(h)}$ for $h = 1, \dots, (H-1)$ using indices $\iota_t^{(h)}$ with $\Pr(\iota_t^{(h)} = h) \propto \zeta_{t-1}^{(h)}$.
(ii) Draw $\tilde{\mathbf{f}}_t^{(h)} | \tilde{\mathbf{f}}_{t-1}^{(\iota_t^{(h)})}, \boldsymbol{\Theta}$ for $h = 1, \dots, (H-1)$ using the state/factor dynamics of the model:

$$\tilde{\mathbf{f}}_t^{(h)} = \mathbf{B} \tilde{\mathbf{f}}_{t-1}^{(\iota_t^{(h)})} + \mathbf{e}_t, \quad \mathbf{e}_t \sim \mathcal{N}(0, \tilde{\mathbf{Q}}).$$

Note that $\tilde{\mathbf{f}}_{t-1}^{(\iota_t^{(h)})}$ denotes the resampled particles from step (i) above.

- (iii) Set the H^{th} particle to the previously accepted draw $\tilde{\mathbf{f}}_t^{(H)} = \tilde{\mathbf{f}}_t^{(s-1)}$.
(iv) Sample $\iota_t^{(H)}$ with probability defined by weights:

$$\Pr(\iota_t^{(H)} = H) \propto \zeta_{t-1}^{(H)} \prod_{\tau=t}^{t-1+\tau_1} g(\mathbf{y}_\tau | \tilde{\mathbf{f}}_{1:t-1}^{(h)}, \tilde{\mathbf{f}}_{t:\tau}^{(s-1)}) f(\tilde{\mathbf{f}}_\tau^{(s-1)} | \tilde{\mathbf{f}}_{1:t-1}^{(h)}, \tilde{\mathbf{f}}_{t:\tau-1}^{(s-1)}).$$

As discussed in Lindsten *et al.* (2014) (see Eq. (23) and Section 7.2 in that paper), this formula is an approximation that can be used when the transition density is degenerate, as in our case. We set the number of lags in this approximation to $\tau_1 = 5$ in our application.

- (v) Update the weights $\zeta_t^{(h)} = \frac{\exp(\tilde{\zeta}_t^{(h)})}{\sum_{k=1}^H \exp(\tilde{\zeta}_t^{(k)})}$, where $\tilde{\zeta}_t^{(h)}$ denotes the conditional log-likelihood.

Sample $\tilde{\mathbf{f}}_t^{(s)}$ with $\Pr(\tilde{\mathbf{f}}_t^{(s)} = \tilde{\mathbf{f}}_t^{(h)}) \propto \zeta_t^{(h)}$ to obtain a draw from the conditional posterior distribution.

2. **Sample unknown parameters in the measurement equation.** Most of the parameters can be sampled on an equation-by-equation basis (i.e., independently over $i = 1, \dots, N$) using well-known conditional posterior distributions. The exception are the GP hyperparameters, which require an equation-specific Metropolis-Hastings (MH) step. Let \star denote conditioning on everything else.

- (i) **Variance of the idiosyncratic components r_i :** Using a conditionally conjugate inverse Gamma prior results in an inverse Gamma conditional posterior of the form:

$$r_i|\star \sim \mathcal{G}^{-1}\left(T + \nu_r, S_r + \frac{\sum_{t=1}^T v_{it}^2}{2}\right), \quad (\text{A.1})$$

with $v_{it} = y_{it} - \sum_{m=1}^M \phi_m(\mathbf{f}_t)c_{im}$.

- (ii) **Coefficients in the observation equation $\mathbf{c}_i = (c_{i1}, \dots, c_{iM})'$:** As shown in Svensson *et al.* (2016), the reduced form approximation outlined in Section 2.3 implies a specific form for the conditional posterior of the coefficients in the observation equation. The conditional posterior is multivariate Gaussian and takes the form:

$$\mathbf{c}_i|\star \sim \mathcal{N}(\bar{\mathbf{c}}_i, \bar{\mathbf{V}}_{\mathbf{c}_i}), \quad (\text{A.2})$$

with

$$\begin{aligned} \bar{\mathbf{V}}_{\mathbf{c}_i} &= \left(\frac{\Phi(\mathbf{F})'\Phi(\mathbf{F})}{r_i} + \underline{\mathbf{V}}_{\mathbf{c}_i}^{-1} \right)^{-1}, \\ \bar{\mathbf{c}}_i &= \bar{\mathbf{V}}_{\mathbf{c}_i} \left(\frac{\Phi(\mathbf{F})'\mathbf{y}_i}{r_i} \right), \end{aligned}$$

where $\underline{\mathbf{V}}_{\mathbf{c}_i} = \text{diag}(\mathcal{S}_i(\sqrt{\lambda_1}), \dots, \mathcal{S}_i(\sqrt{\lambda_M}))$ and $\mathbf{F} = (\mathbf{f}_1, \dots, \mathbf{f}_T)'$.

- (iii) **Kernel parameters $\boldsymbol{\theta}_i$:** To draw $\boldsymbol{\theta}_i$, we use an MH step with a random walk proposal. This amounts to proposing a candidate from

$$\boldsymbol{\theta}_i^* = \exp(\mathbf{s}_{\boldsymbol{\theta}_i}) \boldsymbol{\theta}_i^{(s-1)}, \quad (\text{A.3})$$

with $\mathbf{s}_{\boldsymbol{\theta}_i}$ being sample from a multivariate Gaussian distribution with zero mean and proposal diagonal variance-covariance matrix, set in such a way that the acceptance rate indicates good mixing of this MH step. The acceptance probability is computed as:

$$\min \left(\left[\log p(\boldsymbol{\theta}_i^* | \mathbf{y}_i, \star) + \log q(\boldsymbol{\theta}_i^{(s-1)} | \boldsymbol{\theta}_i^*) - \log p(\boldsymbol{\theta}_i^{(s-1)} | \mathbf{y}_i, \star) - \log q(\boldsymbol{\theta}_i^* | \boldsymbol{\theta}_i^{(s-1)}) \right], 0 \right). \quad (\text{A.4})$$

Here, we evaluate the conditional log-posterior, $\log p(\boldsymbol{\theta}_i | \mathbf{y}_i, \star)$, for both the previously accepted draw $\boldsymbol{\theta}_i^{(s-1)}$ and a candidate value $\boldsymbol{\theta}_i^*$ drawn from the proposal. The conditional log-posterior distribution is straightforward to evaluate and given by: $\log p(\boldsymbol{\theta}_i^* | \mathbf{y}_i, \star) = \log \mathcal{L}(\boldsymbol{\theta}_i) + \log p(\boldsymbol{\theta}_i)$, with $\log \mathcal{L}(\boldsymbol{\theta}_i)$ denoting the log-likelihood and $\log p(\boldsymbol{\theta}_i)$ the log-prior distribution. The conditional log-likelihood is defined as:

$$\log \mathcal{L}(\boldsymbol{\theta}_i) = -\frac{T}{2} \log(2\pi) - \frac{T}{2} \log(r_i(\boldsymbol{\theta}_i)) - \frac{\sum_{t=1}^T v_{it}(\boldsymbol{\theta}_i)^2}{2r_i(\boldsymbol{\theta}_i)},$$

with both $r_i(\boldsymbol{\theta}_i)$ and $v_{it}(\boldsymbol{\theta}_i)$ being a function of the hyperparameters $\boldsymbol{\theta}_i$. The log-prior distribution, $\log p(\boldsymbol{\theta}_i)$ is given by the Gamma distributions outlined in Section 2.4 and a function of the respective hyperparameters ν_ξ , ν_ℓ , S_ξ , and S_ℓ .

3. **Sample unknown parameters in the state equation.** Conditional on knowing \mathbf{f}_t , we sample the parameter in the state equation using the algorithm proposed in [Carriero *et al.* \(2022\)](#).

- (i) The contemporaneous relationships among elements in \mathbf{f}_t (the state equation covariances) can be sampled from conditional (multivariate) Normal posterior distributions. Let $\boldsymbol{\varepsilon}_t = \mathbf{f}_t - \sum_{p=1}^P \mathbf{A}_p \mathbf{f}_{t-p}$ and decompose $\mathbf{Q} = \boldsymbol{\Psi}^{-1} \boldsymbol{\Sigma} (\boldsymbol{\Psi}^{-1})'$ via Cholesky, where $\boldsymbol{\Psi}^{-1}$ is a lower unit triangular matrix and $\boldsymbol{\Sigma} = \text{diag}(\sigma_1^2, \dots, \sigma_D^2)$. In what follows, we can rewrite the system as:

$$\boldsymbol{\Psi} \boldsymbol{\varepsilon}_t = \tilde{\boldsymbol{\varepsilon}}_t, \quad \tilde{\boldsymbol{\varepsilon}}_t \sim \mathcal{N}(\mathbf{0}_D, \boldsymbol{\Sigma}).$$

Using the lower triangular structure of the Cholesky factor, the d^{th} (for $d = 2, \dots, D$) equation resembles a standard regression model:

$$\varepsilon_{dt} = - \sum_{j=1}^{d-1} \psi_{dj} \varepsilon_{jt} + \tilde{\varepsilon}_{dt}, \quad \tilde{\varepsilon}_{dt} \sim \mathcal{N}(0, \sigma_d^2),$$

with ψ_{dj} denoting the $(d, j)^{\text{th}}$ element in $\boldsymbol{\Psi}$. To write such a regression model using full data matrices, let $\boldsymbol{\psi}_d$ denote all free $d - 1$ elements in the d^{th} row of $\boldsymbol{\Psi}$, $\boldsymbol{\varepsilon}_d = (\varepsilon_{d1}, \dots, \varepsilon_{dT})'$, $\tilde{\boldsymbol{\varepsilon}}_d = (\tilde{\varepsilon}_{d1}, \dots, \tilde{\varepsilon}_{dT})'$, and define $\boldsymbol{\varepsilon}_{1:(d-1)} = (\boldsymbol{\varepsilon}_1, \dots, \boldsymbol{\varepsilon}_{(d-1)})$ as a $T \times (d - 1)$ matrix:

$$\boldsymbol{\varepsilon}_d = -\boldsymbol{\varepsilon}_{1:(d-1)} \boldsymbol{\psi}_d + \tilde{\boldsymbol{\varepsilon}}_d, \quad \tilde{\boldsymbol{\varepsilon}}_d \sim \mathcal{N}(\mathbf{0}_T, \boldsymbol{\Xi}_d),$$

with $\boldsymbol{\Xi}_d = \sigma_d^2 \mathbf{I}_T$.² We then draw $\boldsymbol{\psi}_d$ (for $d = 2, \dots, D$) from conditional posterior which is a multivariate Gaussian distribution:

$$\boldsymbol{\psi}_d | \bullet \sim \mathcal{N}(\bar{\boldsymbol{\psi}}_d, \bar{\mathbf{V}}_{\boldsymbol{\psi}_d}).$$

² In case we allow for SV, σ_{dt}^2 varies over time and $\boldsymbol{\Xi}_d = \text{diag}(\sigma_{d1}^2, \dots, \sigma_{dT}^2)$.

Here, $\bar{\boldsymbol{\psi}}_d$ refers to the posterior mean and $\bar{\mathbf{V}}_{\boldsymbol{\psi}_d}$ to the posterior variance, which are given by:

$$\begin{aligned}\bar{\mathbf{V}}_{\boldsymbol{\psi}_d} &= (\boldsymbol{\varepsilon}'_{1:(d-1)} \boldsymbol{\Xi}_d^{-1} \boldsymbol{\varepsilon}_{1:(d-1)} + \mathbf{V}_{\boldsymbol{\psi}_d}^{-1})^{-1}, \\ \bar{\boldsymbol{\psi}}_d &= -\bar{\mathbf{V}}_{\boldsymbol{\psi}_d} (\boldsymbol{\varepsilon}'_{1:(d-1)} \boldsymbol{\Xi}_d^{-1} \boldsymbol{\varepsilon}_d).\end{aligned}$$

$\mathbf{V}_{\boldsymbol{\psi}_d}$ denotes a $(d-1) \times (d-1)$ diagonal prior variance-covariance matrix, with the prior variances on the main diagonal $\underline{\mathbf{v}}_{\boldsymbol{\psi}_d}$ being specific to $\boldsymbol{\psi}_d$. We impose a HS shrinkage prior on these elements. Following [Makalic and Schmidt \(2015\)](#), this implies that the j^{th} element in $\underline{\mathbf{v}}_{\boldsymbol{\psi}_d}$ can be defined as $\underline{v}_{j,\boldsymbol{\psi}_d} = \varpi_{j,\boldsymbol{\psi}_d}^2 \varphi^2$, where $\varpi_{j,\boldsymbol{\psi}_d}^2$, for $j = 1, \dots, (d-1)$, refers to local scales and φ^2 is a single global scale. The global and local scale parameters associated with the HS prior can then be sampled from independent inverse Gamma distributions:

$$\begin{aligned}\varpi_{j,\boldsymbol{\psi}_d}^2 | \star &\sim \mathcal{G}^{-1} \left(1, \frac{1}{\varrho_{j,\boldsymbol{\psi}_d}} + \frac{\psi_{dj}^2}{2\varphi^2} \right), \\ \varphi^2 | \star &\sim \mathcal{G}^{-1} \left(\frac{D(D-1)+2}{4}, \frac{1}{\vartheta} + \sum_{d=1}^D \left(\sum_{j=1}^{d-1} \frac{\psi_{dj}^2}{2\varpi_{j,\boldsymbol{\psi}_d}^2} \right) \right), \\ \varrho_{j,\boldsymbol{\psi}_d} | \star &\sim \mathcal{G}^{-1}(1, 1 + 1/\varpi_{j,\boldsymbol{\psi}_d}^2), \\ \vartheta | \star &\sim \mathcal{G}^{-1}(1, 1 + 1/\varphi^2),\end{aligned}$$

with $\varrho_{j,\boldsymbol{\psi}_d}$ and ϑ denoting auxiliary variables.

(ii) To update the state innovation error variances, we can:

- either sample $\{\sigma_d^2\}_{d=1}^D$ from an inverse Gamma distributions:

$$\sigma_d^2 | \star \sim \mathcal{G}^{-1}(T/2 + 3, \tilde{\boldsymbol{\varepsilon}}'_d \tilde{\boldsymbol{\varepsilon}}_d / 2 + 0.3),$$

- or sample log-volatilities $\{\log \sigma_{dt}^2\}_{d=1}^D$ using the algorithm proposed in [Kastner and Frühwirth-Schnatter \(2014\)](#).

(iii) To sample the reduced form VAR coefficients $\mathbf{A} = (\mathbf{A}_1, \dots, \mathbf{A}_P)$, which is a $D \times K$ -matrix ($K = DP$), on a factor-by-factor basis, we use the updating

step proposed in [Carriero *et al.* \(2022\)](#). Note Eq. (2) can be written as: $\mathbf{f}_t = \mathbf{A}\mathbf{x}_t + \boldsymbol{\varepsilon}_t$, with $\mathbf{x}_t = (\mathbf{f}'_{t-1}, \dots, \mathbf{f}'_{t-P})'$. Let \mathbf{a}_d denote the d^{th} row of \mathbf{A} and $\mathbf{A}_{d=0} = (\mathbf{a}_1, \dots, \mathbf{a}_{d-1}, \mathbf{0}, \mathbf{a}_{d+1}, \dots, \mathbf{a}_D)'$ being an $D \times K$ matrix, in which we zero out the respective d^{th} row in \mathbf{A} . We can manipulate Eq. (2) to isolate \mathbf{a}_d :

$$\Psi(\mathbf{f}_t - \mathbf{A}_{d=0}\mathbf{x}_t) = (\tilde{\boldsymbol{\psi}}_d \otimes \mathbf{x}'_t)\mathbf{a}_d + \tilde{\boldsymbol{\varepsilon}}_t, \quad \tilde{\boldsymbol{\varepsilon}}_t \sim \mathcal{N}(\mathbf{0}_D, \boldsymbol{\Sigma}),$$

with $\tilde{\boldsymbol{\psi}}_d$ denoting the d^{th} column in Ψ . Using the full data matrices, this takes the form of a standard regression model:

$$\ddot{\mathbf{y}}_d = \ddot{\mathbf{X}}_d \mathbf{a}_d + \ddot{\boldsymbol{\varepsilon}}_d, \quad \ddot{\boldsymbol{\varepsilon}}_d \sim \mathcal{N}(\mathbf{0}_{DT}, \ddot{\boldsymbol{\Sigma}}).$$

Here, $\ddot{\mathbf{y}}_d = (\ddot{\mathbf{y}}'_{d1}, \dots, \ddot{\mathbf{y}}'_{dT})'$ is a $DT \times 1$ -vector with the t^{th} element given by $\ddot{\mathbf{y}}_{dt} = \Psi(\mathbf{f}_t - \mathbf{A}_{d=0}\mathbf{x}_t)$, $\ddot{\mathbf{X}}_d = (\mathbf{X} \otimes \tilde{\boldsymbol{\psi}}_d)$ is a $DT \times K$ -matrix with \mathbf{X} collecting \mathbf{x}'_t on the t^{th} row, and $\ddot{\boldsymbol{\Sigma}} = \mathbf{I}_T \otimes \boldsymbol{\Sigma}$ is a $DT \times DT$ diagonal matrix (since $\boldsymbol{\Sigma}$ is diagonal).³ Note both $\ddot{\mathbf{y}}_d$ and $\ddot{\mathbf{X}}_d$ are factor-specific and therefore feature a d subscript. For $d = 1, \dots, D$, we can then draw \mathbf{a}_d from a multivariate Gaussian conditional posterior distribution:

$$\mathbf{a}_d | \bullet \sim \mathcal{N}(\bar{\mathbf{a}}_d, \bar{\mathbf{V}}_{\mathbf{a}_d}),$$

with $\bar{\mathbf{a}}_d$ referring to the posterior mean and $\bar{\mathbf{V}}_{\mathbf{a}_d}$ to the posterior variance. The two posterior moments are given by:

$$\begin{aligned} \bar{\mathbf{V}}_{\mathbf{a}_d} &= \left(\ddot{\mathbf{X}}_d' \ddot{\boldsymbol{\Sigma}}^{-1} \ddot{\mathbf{X}}_d + \underline{\mathbf{V}}_{\mathbf{a}_d}^{-1} \right)^{-1}, \\ \bar{\mathbf{a}}_d &= \bar{\mathbf{V}}_{\mathbf{a}_d} \left(\ddot{\mathbf{X}}_d' \ddot{\boldsymbol{\Sigma}}^{-1} \ddot{\mathbf{y}}_d \right). \end{aligned}$$

$\underline{\mathbf{V}}_{\mathbf{a}_d}$ is a $K \times K$ diagonal prior variance-covariance matrix, with the prior variances on the main diagonal $\underline{\mathbf{v}}_{\mathbf{a}_d}$ being specific to \mathbf{a}_d . Similarly, to the contem-

³ $\ddot{\boldsymbol{\Sigma}} = \mathbf{I}_T \otimes \boldsymbol{\Sigma}$ in case of homoskedastic VAR errors. If we allow for heteroskedastic errors, we have $\ddot{\boldsymbol{\Sigma}} = \text{diag}(\sigma_{11}, \dots, \sigma_{D1}, \dots, \sigma_{1T}, \dots, \sigma_{DT})$.

poraneous relationships, we use a HS prior for \mathbf{a}_d . This implies $\underline{v}_{j,\mathbf{a}_d} = \varpi_{j,\mathbf{a}_d}^2 \varphi_{\mathbf{a}_d}^2$, where $\varpi_{j,\mathbf{a}_d}^2$, for $j = 1, \dots, K$, are local scales and $\varphi_{\mathbf{a}_d}^2$ is an factor-specific global scale. We have the following independent inverse Gamma conditional posterior distributions:

$$\begin{aligned}\varpi_{j,\mathbf{a}_d}^2 | \star &\sim \mathcal{G}^{-1} \left(1, \frac{1}{\varrho_{j,\mathbf{a}_d}} + \frac{a_{dj}^2}{2\varphi_{\mathbf{a}_d}^2} \right), \\ \varphi_{\mathbf{a}_d}^2 | \star &\sim \mathcal{G}^{-1} \left(\frac{K+1}{2}, \frac{1}{\vartheta_{\mathbf{a}_d}} + \sum_{j=1}^K \frac{a_{dj}^2}{2\varpi_{j,\mathbf{a}_d}^2} \right), \\ \varrho_{j,\mathbf{a}_d} | \star &\sim \mathcal{G}^{-1}(1, 1 + 1/\varpi_{j,\mathbf{a}_d}^2), \\ \vartheta_{\mathbf{a}_d} | \star &\sim \mathcal{G}^{-1}(1, 1 + 1/\varphi_{\mathbf{a}_d}^2),\end{aligned}$$

with ϱ_{j,\mathbf{a}_d} and $\vartheta_{\mathbf{a}_d}$ denoting auxiliary variables.

B. DATA APPENDIX

Table B.1: List of FRED-QD variables used in the forecasting exercise.

FRED MNEMONIC	Description	Transformation
GDPC1	Real Gross Domestic Product	(5)
PAYEMS	All Employees: Total Nonfarm	(5)
CPIAUCSL	Consumer Price Index: All Items	(6)
FEDFUNDS	Effective Federal Funds Rate	(2)
PCDGx	Real Personal Consumption Expenditures: Durable Goods	(5)
PCESVx	Real Personal Consumption Expenditures: Services	(5)
PCNDx	Real Personal Consumption Expenditures: Nondurable Goods	(5)
Y033RC1Q027SBEAx	Real Gross Private Domestic Investment: Fixed Investment (Nonresidential)	(5)
PNFIx	Real Private Fixed Investment: Nonresidential	(5)
PRFIx	Real Private Fixed Investment: Residential	(5)
A014RE1Q156NBEA	Shares of Gross Domestic Product: Gross Private Domestic Investment (Change in Private Inventories)	none
A823RL1Q225SBEA	Real Government Consumption Expenditures and Gross Investment (Federal)	none
FGRECPTx	Real Federal Government Current Receipts	(5)
SLCEx	Real Government State and Local Consumption Expenditures	(5)
EXPGSC1	Real Exports of Goods & Services	(5)
IMPGSC1	Real Imports of Goods & Services	(5)
IPDMAT	Industrial Production: Durable Materials	(5)
IPNMAT	Industrial Production: Nondurable Materials	(5)
IPDCONGD	Industrial Production: Durable Consumer Goods	(5)
IPB51110SQ	Industrial Production: Durable Goods – Automotive Products	(5)
IPNCONGD	Industrial Production: Nondurable Consumer Goods	(5)
IPBUSEQ	Industrial Production: Business Equipment	(5)
IPB51220SQ	Industrial Production: Consumer Energy Products	(5)
CUMFNS	Capacity Utilization: Manufacturing (SIC)	none
DMANEMP	All Employees: Durable Goods	(5)
USCONS	All Employees: Construction	(5)
USEHS	All Employees: Education & Health Services	(5)
USFIRE	All Employees: Financial Activities	(5)
USINFO	All Employees: Information Services	(5)

Transformation codes: (2) Δx_t , (5) $\Delta \log(x_t)$, (6) $\Delta^2 \log(x_t)$; continued on next page

Table B.1 – continued from previous page

FRED MNEMONIC	Description	Transformation
USPBS	All Employees: Professional & Business Services	(5)
USLAH	All Employees: Leisure & Hospitality	(5)
USSERV	All Employees: Other Services	(5)
USMINE	All Employees: Mining and Logging	(5)
USTPU	All Employees: Trade, Transportation & Utilities	(5)
USTRADE	All Employees: Retail Trade	(5)
USWTRADE	All Employees: Wholesale Trade	(5)
CES9091000001	All Employees: Government – Federal	(5)
CES9092000001	All Employees: Government – State Government	(5)
CES9093000001	All Employees: Government – Local Government	(5)
LNS14000012	Unemployment Rate – 16 to 19 Years	(2)
LNS14000025	Unemployment Rate – 20 Years and over, Men	(2)
LNS14000026	Unemployment Rate – 20 Years and over, Women	(2)
UEMPLT5	Number of Civilians Unemployed – Less Than 5 Weeks	(5)
UEMP5TO14	Number of Civilians Unemployed for 5 to 14 Weeks	(5)
UEMP15T26	Number of Civilians Unemployed for 15 to 26 Weeks	(5)
UEMP27OV	Number of Civilians Unemployed for 27 Weeks and Over	(5)
LNS12032194	Employment Level – Part-Time for Economic Reasons, All Industries	(5)
AWHMAN	Average Weekly Hours of Production and Nonsupervisory Employees: Manufacturing	none
AWHNONAG	Average Weekly Hours Of Production And Nonsupervisory Employees: Total Private	(2)
AWOTMAN	Average Weekly Overtime Hours of Production and Nonsupervisory Employees: Manufacturing	(2)
PERMIT	New Private Housing Units Authorized by Building Permits	(5)
HOUSTMW	Housing Starts in Midwest Census Region	(5)
HOUSTNE	Housing Starts in Northeast Census Region	(5)
HOUSTS	Housing Starts in South Census Region	(5)
HOUSTW	Housing Starts in West Census Region	(5)
AMDMNOx	Real Manufacturers' New Orders: Durable Goods	(5)
AMDMUOx	Real Value of Manufacturers' Unfilled Orders for Durable Goods Industries	(5)
GPDICTPI	Gross Private Domestic Investment: Chain-type Price Index	(6)
IPDBS	Business Sector: Implicit Price Deflator	(6)
DMOTRG3Q086SBEA	Personal Consumption Expenditures: Durable Goods – Motor Vehicles and Parts	(6)
DFDHRG3Q086SBEA	Personal Consumption Expenditures: Durable Goods – Furnishings and Durable Household Equipment	(6)
DREQRG3Q086SBEA	Personal Consumption Expenditures: Durable Goods – Recreational Goods and Vehicles	(6)
DODGRG3Q086SBEA	Personal Consumption Expenditures: Durable Goods – Other Durable Goods	(6)
DFXARG3Q086SBEA	Personal Consumption Expenditures: Nondurable Goods – Food and Beverages Purchased for Off-Premises Consumption	(6)

Transformation codes: (2) Δx_t , (5) $\Delta \log(x_t)$, (6) $\Delta^2 \log(x_t)$; continued on next page

Table B.1 – continued from previous page

FRED MNEMONIC	Description	Transformation
DCLOGRG3Q086SBEA	Personal Consumption Expenditures: Nondurable Goods – Clothing and Footwear	(6)
DGOERG3Q086SBEA	Personal Consumption Expenditures: Nondurable Goods – Gasoline and Other Energy Goods	(6)
DONGRG3Q086SBEA	Personal Consumption Expenditures: Nondurable Goods – Other Nondurable Goods	(6)
DHUTRG3Q086SBEA	Personal Consumption Expenditures: Services – Housing and Utilities	(6)
DHLCRG3Q086SBEA	Personal Consumption Expenditures: Services – Health care (chain-type price index)	(6)
DTRSRG3Q086SBEA	Personal Consumption Expenditures: Transportation Services	(6)
DRCARG3Q086SBEA	Personal Consumption Expenditures: Recreation Services	(6)
DFSARG3Q086SBEA	Personal Consumption Expenditures: Services – Food Services and Accommodations	(6)
DIFSRG3Q086SBEA	Personal Consumption Expenditures: Financial Services and Insurance	(6)
DOTSRG3Q086SBEA	Personal Consumption Expenditures: Other Services	(6)
WPSFD49502	Producer Price Index by Commodity for Final Demand: Personal Consumption Goods (Finished Consumer Goods)	(6)
WPSFD4111	Producer Price Index by Commodity for Finished Consumer Foods	(6)
PPIIDC	Producer Price Index by Commodity Industrial Commodities	(6)
WPSID61	Producer Price Index by Commodity Intermediate Materials: Supplies & Components	(6)
WPU0561	Producer Price Index by Commodity for Fuels and Related Products and Power: Crude Petroleum (Domestic Production)	(5)
COMPRNFB	Nonfarm Business Sector: Real Compensation Per Hour	(5)
RCPHBS	Business Sector: Real Compensation Per Hour	(5)
OPHNFB	Nonfarm Business Sector: Real Output Per Hour of All Persons	(5)
ULCNFB	Nonfarm Business Sector: Unit Labor Cost	(5)
UNLPNBS	Nonfarm Business Sector: Unit Nonlabor Payments	(5)
TB3MS	3-Month Treasury Bill: Secondary Market Rate	(2)
BAA10YM	Moody's Seasoned Baa Corporate Bond Yield Relative to Yield on 10-Year Treasury Constant Maturity	none
TB6M3Mx	6-Month Treasury Bill Minus 3-Month Treasury Bill	none
GS1TB3Mx	1-Year Treasury Constant Maturity Minus 3-Month Treasury Bill	none
GS10TB3Mx	10-Year Treasury Constant Maturity Minus 3-Month Treasury Bill	none
BUSLOANSx	Real Commercial and Industrial Loans, All Commercial Banks	(5)
CONSUMERx	Real Consumer Loans at All Commercial Banks	(5)
NONREVSLx	Total Real Nonrevolving Credit Owned and Securitized, Outstanding	(5)
REALLNx	Real Real Estate Loans, All Commercial Banks	(5)
TLBSHNOx	Real Total Liabilities of Households and Nonprofit Organizations	(5)
TNWBSHNOx	Real Net Worth of Households and Nonprofit Organizations	(5)
TARESAx	Real Assets of Households and Nonprofit Organizations excluding Real Estate Assets	(5)
HNOREMQ027Sx	Real Real Estate Assets of Households and Nonprofit Organizations	(5)
TFAABSHNOx	Real Total Financial Assets of Households and Nonprofit Organizations	(5)
VIXCLSx	CBOE Volatility Index	(5)

Transformation codes: (2) Δx_t , (5) $\Delta \log(x_t)$, (6) $\Delta^2 \log(x_t)$; continued on next page

Table B.1 – continued from previous page

FRED MNEMONIC	Description	Transformation
EXSZUSx	Switzerland / US Foreign Exchange Rate	(5)
EXJPUSx	Japan / US Foreign Exchange Rate	(5)
EXUSUKx	UK / US Foreign Exchange Rate	(5)
EXCAUSx	Canada / US Foreign Exchange Rate	(5)
UMCSENTx	University of Michigan: Consumer Sentiment	none
SP500	S&P 500 Common Stock Price Index: Composite	(5)

Transformation codes: (2) Δx_t , (5) $\Delta \log(x_t)$, (6) $\Delta^2 \log(x_t)$